

May 08, 2020

Dear Editor Prof. Fangqun Yu,

On behalf of all co-authors, we would like to thank you for your help on handling our manuscript entitled "Effects of continental emissions on Cloud Condensation Nuclei (CCN) activity in northern South China Sea during summertime 2018". We also want to thank the referees for valuable comments and suggestions on the manuscript. We believe that we have addressed all the concerns raised by referees. Enclosed in this letter are our point-by-point responses to the referees' comments (in blue) and changes made in the revision (in red). We hope our revised manuscript would be satisfactory for acceptance. Again, thank you very much for your time and efforts on handling our manuscript. We are looking forward to hearing from you soon!

Yours sincerely,

Jun Zhao, Prof./PhD

Haobo Tan, Prof./PhD

Reply to reviewer #1' comments

We would like to thank the reviewer for valuable comments and suggestions. We have addressed all raised issues in the revision accordingly. Please kindly find our following point-by-point responses (the reviewer's comments in black, our responses in blue, and relevant changes in red).

Major comments:

1. The authors mention that they removed abnormal measurement spikes from their data set. They attribute these spikes to potential interference from their ship or other ships' emissions. This seems rather arbitrary way of throwing out data without more concrete reasoning. Can the authors provide chemical analysis of particles found in these spikes? Does the composition match what is expected for ship exhaust? Also, does the wind direction correlate with when ship emission would impact the container of instruments? How long did these spikes last? How many spikes in the data were there (hard to tell from the Figure S1)? Were the spikes just removed or averaged out? It would be helpful to actually reference the supplemental figures in the main text so the reader knows what the raw data of NCN looked like. The authors point out that shipping emission likely contribute significantly to particles in the South China Sea (line 120). Why then would the authors throw out observations from shipping emissions? In short, the authors must better justify why these spikes in data were thrown out and to know more definitively what was causing these spikes.

Reply:

We thank the reviewer for commenting on processing the abnormal spikes. We have added the temporal profiles of aerosol chemical composition, NO/NO₂/NO_x, along with wind direction and speed in Figure S1. Before removing the abnormal data, the spikes appear simultaneously in N_{CN} (d), organics (f) and NO/NO₂/NO_x (g). There are mainly three potential sources: 1) emissions from our ship and other adjacent ships; 2) emissions from the kitchen in our ship; 3) smoking from sailors in our ship (It is really unfortunate, however, smoking did happen frequently during the measurements). It is difficult to distinguish those sources without detailed

source apportionment. As we focus on cloud condensation nuclei (CCN) activity, we do not intend to apportion sources of organic matter in this paper and detailed organic source apportionment will be the focus of our next paper.

We measure NO/NO₂/NO_x every minute in comparison to 5 and 15 min per cycle respectively for the CCN and ToF-ACSM measurements. Hence more spikes could be found in the profiles of NO/NO₂/NO_x than in organic composition from the ToF-ACSM measurements. A total number of about 30, 40, 50 spikes were found in the profiles of organic composition, N_{CCN}, and NO/NO₂/NO_x, respectively.

The weather station was placed on the rooftop of the cockpit which was located in the front of the ship. Wind direction and speed measured by the weather station was shown in Figure S1 (a, b). Note that the wind direction and speed are relative to those of the ship because it sailed most of the time during the measurements. Hence corrections are needed for accurate determination of the absolute wind direction and speed, which needs high temporal resolution and precise records on the direction and speed of the ship. Unfortunately, such records are not available during the measurements. Nevertheless, the spikes do not correspond significantly to changes of the wind direction and speed as shown in Fig. S1.

The spikes could last from minutes to hours. If they are from smoking, then they could last a few minutes. In some cases, if other ships sailed adjacently (i.e., within a few hundred meters) in the same direction, emissions from those ships could cause spikes that would last a few hours. When the ship anchored, emissions from the ship itself could cause spikes as well. In this study, the protocol for removal of spikes is to keep as many data as we can while avoiding too complicated data processing. We argue that ship emission could be one of the major particle sources in the South China Sea region. Here ship emission should be regional representative, rather than emissions from the ship itself and emissions from other adjacent ships which are really close to the measurement ship (i.e., within several hundred meters) because those emissions could cause extreme heterogeneity of spatial distributions. Hence those emissions should be excluded from further data analysis. Base on the above rationales, we remove all the spikes associated with smoking, emissions from the ship and from other adjacent ships, and emissions from the kitchen on the ship. We have also included concentrations of chemical composition and NO/NO₂/NO_x before and after removal in Fig. S1 for comparison. We believe

that removal of the spikes based on the proposed protocol would not significantly affect our conclusions on the CCN activity in this study.

We have now added several sentences on p14 (L278-282) in the revision, “For consistency, we removed spikes likely associated with smoking, emissions from the ship itself and other adjacent ships and cooking from further data analysis, including either abrupt high number concentrations of particles (measured by SMPS), organics (measured by ToF-ACSM), and NO_x (measured by the NO_x monitor) (Detailed criteria can be referred to descriptions and Fig. S1 in supplementary).”

We have also included a paragraph of detailed descriptions regarding how to remove spikes from the data in supplementary.

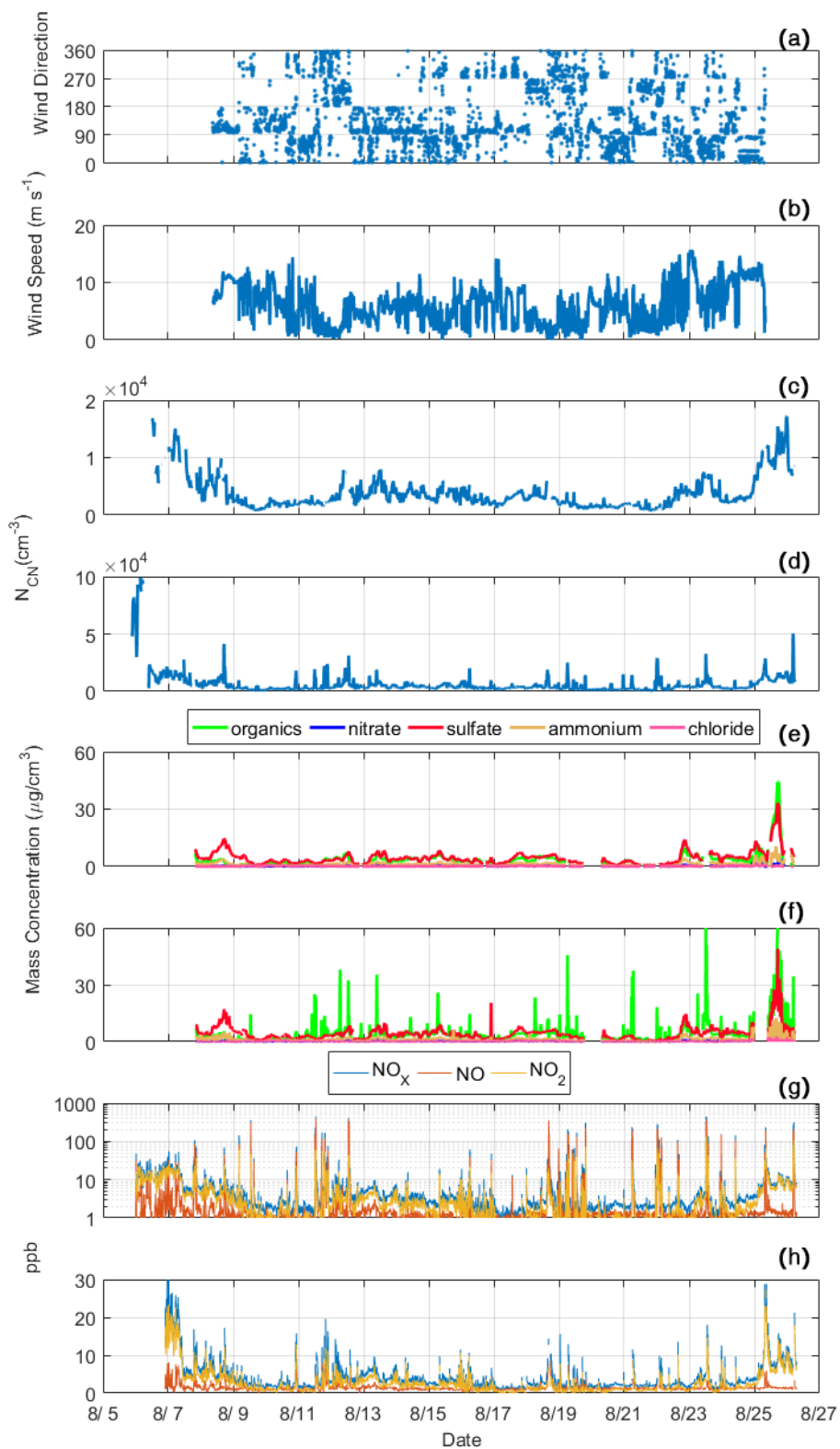


Figure S1. Temporal profile of wind direction (a) and wind speed (b), N_{CN} after (c) and before (d) removal of the abnormal data, chemical composition after (e) and before (f), and $NO/NO_2/NO_x$ before (g) and after (h) removal of the abnormal data.

2. Line 270: authors attribute high sulfate content to ship emissions instead of oxidation of DMS from ocean. Can the authors estimate sulfur emissions from the ocean from previous studies and compare that to what they saw? This would provide more solid evidence that the elevated sulfate content is due to ship emissions than from ocean DMS.

Reply:

We thank the reviewer for valuable suggestions on sulfate formation. Possible sources of sulfate include ship emissions, DMS oxidation, and transport from inland etc. The oxidation of DMS leads to formation of sulfur dioxide and methansulfonic acid (MSA) both of which can be further oxidized to produce non-sea-salt (NSS) sulfate in marine atmosphere. Oxidation of SO₂ from ship emissions or inland transport can also be a major source of NSS sulfate (Savoie et al., 2002). As an intermediate between DMS and sulfate, MSA in principle can be detected by ToF-ACSM, although resolution of the instrument is low. We are currently working on MSA identification and quantification from this cruise measurement. Preliminary results show that the fraction of sulfate from DMS oxidation is far below that from ship emissions. An early study showed that anthropogenic sulfate accounted for about 81-97% of NSS sulfate over China Sea (Guo et al., 1996). A ratio of 15-655 NSS sulfate to MSA in PM_{2.5} was reported in the Northern South China Sea (Zhang et al., 2007), much higher than that (18-20) in the remote marine (Savoie et al., 2002). Here we employed the Modern-Era Retrospective analysis for Research and Applications, Version 2 (MERRA-2) to analyze the distribution of ratio of sulfate to MSA at 925 hPa during the measurement period. The results were shown in Fig. S2 and the ratio ranged from 100 to 10000 over the SCS, much higher than that in the remote Pacific Ocean (1-50). In addition, it also increases with latitude, indicating that the anthropogenic emission is the major source of the total sulfate in the Northern SCS region.

To be clarified, we have added several sentences to discuss the origin of sulfate on p13-14 (L257-270) in the revision, “The oxidation of DMS leads to formation of sulfur dioxide and methansulfonic acid (MSA) both of which can be further oxidized to produce non-sea-salt (NSS) sulfate in marine atmosphere. Oxidation of SO₂ from ship emissions or inland transport can also be a major source of NSS sulfate (Savoie et al., 2002). As an intermediate between DMS and sulfate, MSA in principle can be detected by ToF-ACSM, although resolution of the instrument is low. Preliminary results show that the fraction of sulfate from DMS oxidation is

far below that from ship emissions. An early study showed that anthropogenic sulfate accounted for about 81-97% of NSS sulfate over China Sea (Gao et al., 1996). A ratio of 15-655 NSS sulfate to MSA in $PM_{2.5}$ was reported in the northern South China Sea (Zhang et al., 2007), much higher than that (18-20) in the remote marine (Savoie et al., 2002). Here we employed the Modern-Era Retrospective analysis for Research and Applications, Version 2 (MERRA-2) to analyze the distribution of ratio of sulfate to MSA at 925 hPa during the measurement period (GMAO, 2015). The results were shown in Fig. S2 and the ratio ranged from 100 to 10000 over the SCS, much higher than that in the remote Pacific Ocean (1-50). In addition, it also increases with latitude, indicating that the anthropogenic emission is likely the major source of the total sulfate in the northern SCS region.”

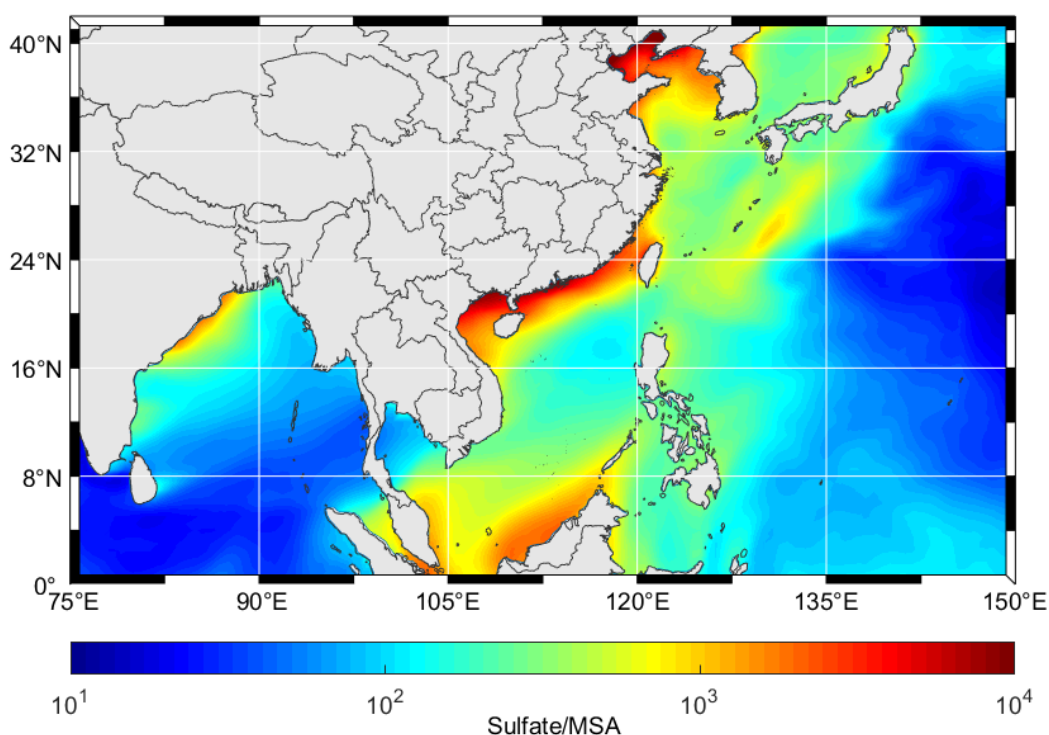


Figure S2. The ratio of sulfate to MSA at 925 hPa from MERRA-2 reanalysis dataset (GMAO, 2015).

Minor Comments:

1. Abstract seems unnecessarily long. Would be more readable if it were shortened to include the main point of the paper.

Reply:

We have modified the abstract as follows, “Aerosol particles in marine atmosphere have been shown to significantly affect cloud formation, atmospheric optical properties, and climate change. However, high temporally and spatially resolved atmospheric measurements over sea are currently sparse, limiting our understanding of aerosol properties in marine atmosphere. In this study, a ship-based cruise campaign was conducted over northern South China Sea (SCS) region during summertime 2018. Chemical composition of non-refractory PM₁ (NR-PM₁), particle number size distribution (PNSD) and size-resolved cloud condensation nuclei (CCN) activity were measured by a time-of-flight aerosol chemical speciation monitor (ToF-ACSM), and the combination of a cloud condensation nuclei counter (CCNc) and a scanning mobility particle sizer (SMPS), respectively. Overall, aerosol particles exhibited a unimodal distribution centering at 60~80 nm and chemical composition of the NR-PM₁ was dominated by sulfate (~46%) which likely originated from anthropogenic emissions rather than dimethyl sulfide (DMS) oxidation. Two polluted episodes were respectively observed at the beginning (P1) and at the end (P2) of the campaign and both were characterized by high particle number concentrations (N_{CN}) which originated respectively from local emissions and from emissions in inland China via long range transport as shown by back trajectory analysis. The concentrations of trace gases (i.e., O₃, CO, NO_x) and particles (N_{CN} and N_{CCN} at ss=0.34%) were elevated during P2 and decrease with the offshore distance, further suggesting important impacts of anthropogenic emissions from the inland Pearl River Delta (PRD) region on the northern SCS. Two relatively clean periods (C1 and C2) prior to and after tropical storm Bebinca were classified due to substantial removal of pollutants by strong winds and rainfalls accompanying with the storm. During C1 and C2 periods, the air was affected by air masses from southwest and from Indo-China Peninsula, respectively. Chemical composition measurements showed an increase of organic mass fraction during P2 compared to C2; however, no obviously different κ values were obtained from the CCNc measurements, implying that the air masses carried pollutants from local sources during long range transport. We report an average value of about 0.4 for aerosol hygroscopicity parameter κ which falls within the literature values (i.e., 0.2-1.0) for urban and remote marine atmosphere. In addition, our results showed that the CCN fraction (N_{CCN}/N_{CN,tot}) and the κ values obtained from the CCNc

measurements (ss=0.34%) had no clear correlation either with the offshore distance or with concentrations of the particles. Our study highlights dynamical variations of particle properties and the impact of long range transport from the China continent and Indo-China Peninsula on the northern SCS region during summertime.”

2. Line 21: high temporally and spatially resolved

Reply: The sentence has been revised to “...high temporally and spatially resolved” in the abstract.

3. Line 82: how was mixing state important for CCN? If it's important, why did the authors not address how mixing state may impact their measurements conclusions?

Reply:

Mixing state of particles has important impact on CCN prediction based on chemical composition and D_{50} if the measurements were significantly affected by primary emissions, since the above methods for CCN prediction assume particles to be internally mixed. Freshly emitted black carbon (BC) particles are externally mixed and hydrophobic, hence they are hard to be activated as CCN. However, aged BC particles coated with inorganic matter will become internally mixed and CCN activated. In addition, mixing state of particles can also affect the shape of activation curves. For externally mixed particles, their activation curves are usually smooth (Cai et al., 2018).

We have plotted the activation curves at 0.18% ss during the four periods (P1, P2, C1, and C2) as shown in Fig. S4 in supplementary and have added a paragraph to discuss mixing state on p21-22 (L429-441) in the revision, “The mixing state and heterogeneity of particles can affect the steepness of the activation curves (Cai et al., 2018). A steeper curve indicates that particles intend to be internally mixed and have a higher similarity in hygroscopicity. The average activation curves at 0.18% SS during the P1, C1, C2 and P2 periods are shown in Fig. S4. The parameter C (in Eq. 1) can be used to present the steepness of activation curve. A small C value indicates a steep activation curve. The C values during P1, C1, C2 and P2 periods were -8.5, -14.3, -13.7 and -10.6, respectively. The smooth curve and the largest C value during P1 suggest that particles had a higher degree of external mixing and higher heterogeneity, owing to the

local fresh emissions. The C values during C1 and C2 periods were close and smaller than those in pollution periods, implying particles during clean periods were more aged and tend to be more internally mixed. The backward trajectories show that the air masses during clean periods were less affected by fresh emissions. The activation curve during P2 period was smoother than C1 and C2 but steeper than P1, indicating that the particles during this period could be a mixture of aged particles from China inland and fresh particles from onshore emissions.”

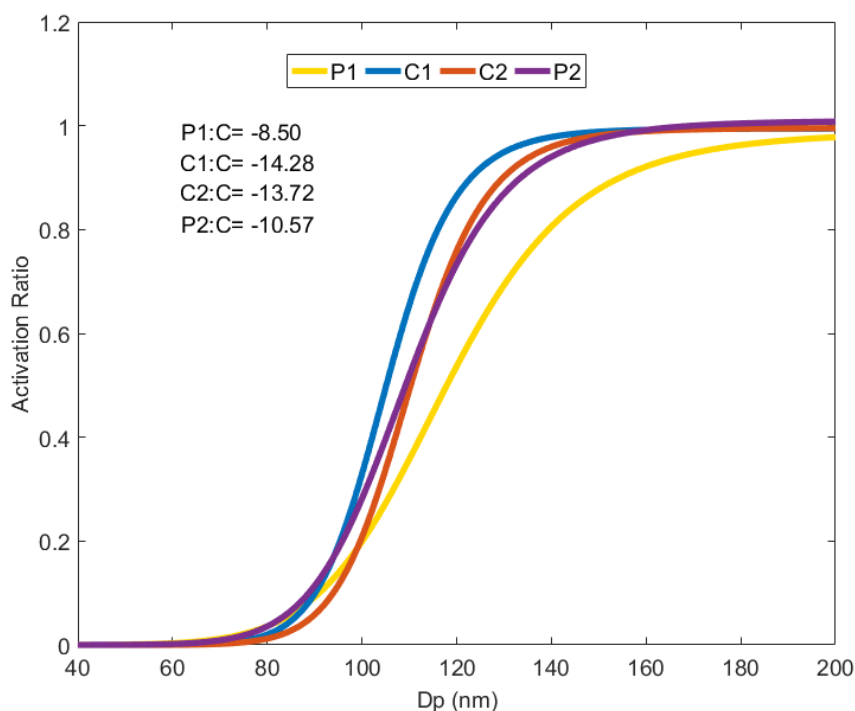


Figure S4. The activation curve at 0.18% ss during the P1, C1, C2 and P2 periods. Different colors represent different periods.

4. Line 102: unclear the sentence starting with Furthermore.

Reply: “Furthermore” has been replaced by “Meanwhile” on p6 (L95)

5. Line 148: delete both

Reply: deleted.

6. Line 149: comma before which

Reply: A comma has been added.

7. Line 161: “, which is listed in Table 1,”

Reply: The sentence has been revised.

8. Line 213: remove firstly

Reply: Removed.

9. Line 299: please use parallel phrasing for this sentence.

Reply: This sentence has been revised on p15 (L299-301) in the revision to “Comparison of the hygroscopicity parameter κ obtained from this study, urban Guangzhou, remote marine Okinawa, remote South China Sea, and mountain Goldlauter was shown in Fig. 3.”

10. Line 385: was likely

Reply: It has been revised.

11. Line 405: if the particles are from biomass burning, do the authors observe any of the classic biomass burning tracers (such as K)?

Reply:

The K can be a tracer of biomass burning and sea salt. However, the vaporizer of ACSM and AMS can produce a large amount of K^+ , which will interfere the ambient K signal. To our knowledge, there could be a large uncertainty of the K concentration measured by ACSM. The levoglucosan can also be the tracer of biomass burning. Nevertheless, the mass resolution of our ACSM is too low to distinguish levoglucosan from other species. Currently, there are no direct evidences indicating the impact of biomass burning. We analyzed fire detection data during the measurements from MODIS in combination with back trajectories during C2 which clearly show that the air parcels pass through the fire region. We have modified Fig. 7 and added a discussion on p20 (L407-410), “The backward trajectories during C2 pass through the burning regions in Southeast Asia (e.g., Viet Nam, Laos, Cambodia etc.), also supporting this conjecture.

However, more solid evidences are needed since the observation of biomass burning tracers (such as K and levoglucosan) is missing in this campaign.”

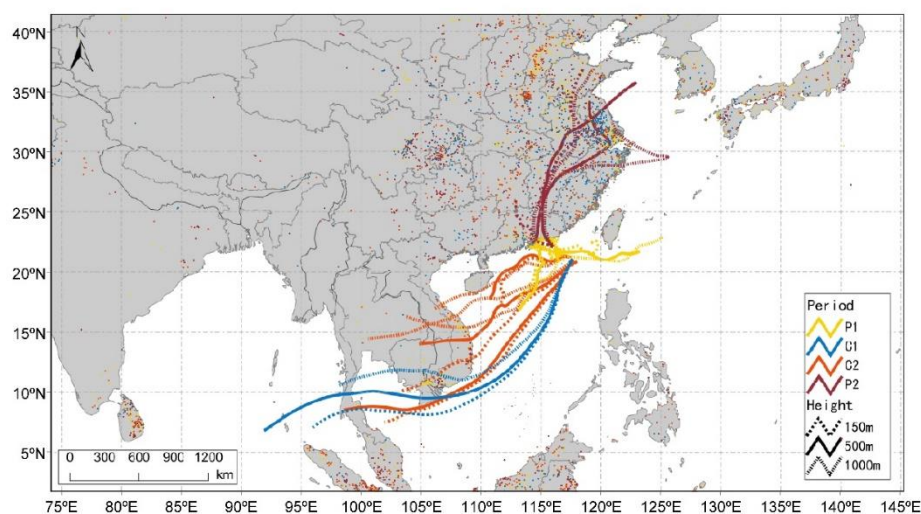


Figure 7. The 72 h backward trajectories arriving at the location of the vessel with three heights (150 m, 500 m, and 1000 m) during P1, C1, C2, and P2, respectively. The dots represent the fire spots detected by MODIS.

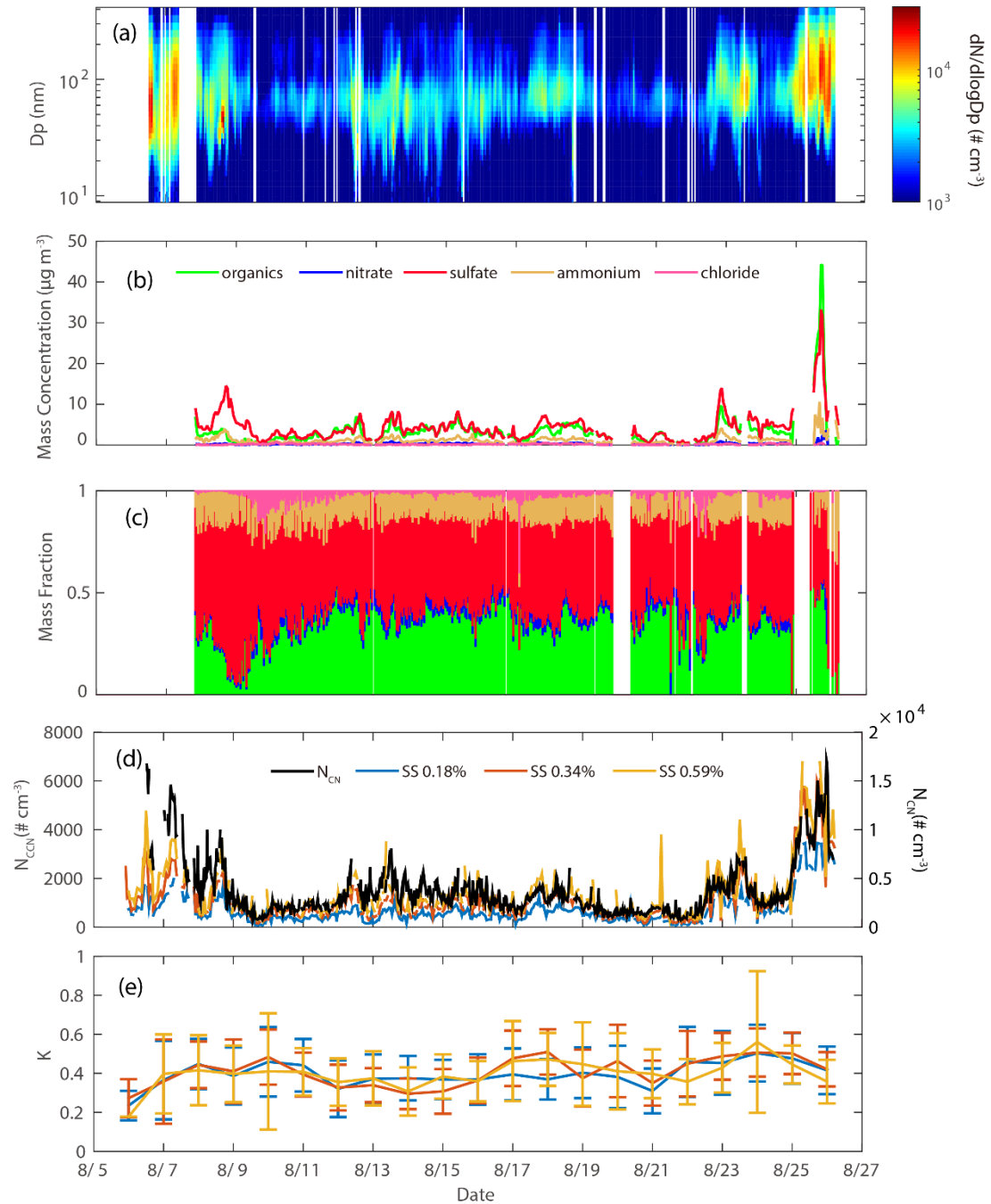
12. Table 2: the values have too many significant figures given the uncertainties of the measurement

Reply: Table 2 has been revised.

| Period | ss | 0.18% | 0.34% | 0.59% |
|--------|--------------------------------|-------|-------|-------|
| P1 | $N_{CCN} (\# \text{ cm}^{-3})$ | 1825 | 3969 | 7198 |
| | $D_{50} (\text{nm})$ | 132 | 96 | 65 |
| | $N_{CCN}/N_{CN,tot}$ | 0.19 | 0.34 | 0.49 |
| C1 | $N_{CCN} (\# \text{ cm}^{-3})$ | 566 | 978 | 1330 |
| | $D_{50} (\text{nm})$ | 105 | 67 | 49 |
| | $N_{CCN}/N_{CN,tot}$ | 0.31 | 0.54 | 0.71 |
| C2 | $N_{CCN} (\# \text{ cm}^{-3})$ | 536 | 844 | 1183 |
| | $D_{50} (\text{nm})$ | 108 | 68 | 48 |
| | $N_{CCN}/N_{CN,tot}$ | 0.32 | 0.55 | 0.73 |
| P2 | $N_{CCN} (\# \text{ cm}^{-3})$ | 4969 | 7140 | 8679 |
| | $D_{50} (\text{nm})$ | 101 | 65 | 49 |
| | $N_{CCN}/N_{CN,tot}$ | 0.49 | 0.74 | 0.85 |

13. Figure 2d) what is the black line? And which lines go to which y axis?

Reply: The black line represents the N_{CN} , corresponding to the y axis on the right. The rest represents the N_{CCN} at different ss, corresponding to the left axis. Figure 2 has been modified.



References:

- Cai, M., Tan, H., Chan, C. K., Qin, Y., Xu, H., Li, F., Schurman, M. I., Liu, L., and Zhao, J.: The size-resolved cloud condensation nuclei (CCN) activity and its prediction based on aerosol hygroscopicity and composition in the Pearl Delta River (PRD) region during wintertime 2014, *Atmos. Chem. Phys.*, 18, 16419-16437, 2018.
- Gao, Y., Arimoto, R., Duce, R. A., Chen, L. Q., Zhou, M. Y., and Gu, D. Y.: Atmospheric non-sea-salt sulfate, nitrate and methanesulfonate over the China Sea, *J. Geophys. Res. Atmos.*, 101, 12601-12611, 10.1029/96jd00866, 1996.
- Global Modeling and Assimilation Office (GMAO) (2015), MERRA-2 inst3_3d_aer_Nv: 3d,3-Hourly,Instantaneous,Model-Level,Assimilation,Aerosol Mixing Ratio V5.12.4, Greenbelt, MD, USA, Goddard Earth Sciences Data and Information Services Center (GES DISC), Accessed: 8, 2018, 10.5067/LTVB4GPCOTK2.
- Savoie, D. L., Arimoto, R., Keene, W. C., Prospero, J. M., Duce, R. A., and Galloway, J. N.: Marine biogenic and anthropogenic contributions to non-sea-salt sulfate in the marine boundary layer over the North Atlantic Ocean, *J. Geophys. Res. Atmos.*, 107, AAC 3-1-AAC 3-21, 10.1029/2001JD000970, 2002.
- Zhang, X., Zhuang, G., Guo, J., Yin, K., and Zhang, P.: Characterization of aerosol over the Northern South China Sea during two cruises in 2003, *Atmos. Environ.*, 41, 7821-7836, 2007.

Reply to reviewer #2' comments

We would like to thank the reviewer for valuable comments and suggestions. We have addressed all raised issues in the revision accordingly. Please kindly find our following point-by-point responses (the reviewer's comments in black, our responses in blue, and relevant changes in red).

1. The manuscript is quite difficult to follow as it is just describing a lengthy dataset by correlating each other. It is highly unclear what is the main scientific conclusions of the data analysis. This issue is well represented in the lengthy abstract of the manuscript. It is just way too long, which makes difficult to grasp the scientific merits of data analysis. I strongly recommend the authors to remind themselves a couple of main scientific findings that they hope to come across in the manuscript for the revision.

Reply:

We thank the reviewer for valuable suggestions. As we state in the abstract, aerosol particles in marine atmosphere can significantly affect cloud formation, atmospheric optical properties, and climate change. Currently, high temporally and spatially resolved atmospheric measurements over sea are sparse, limiting our knowledge on understanding of aerosol properties in marine atmosphere. We utilized measurement data from a recent ship-based cruise campaign to analyze the CCN activity over the northern South China Sea and to investigate the effects of continental emissions on the CCN activity. We agree with the reviewer that the abstract should be concise and we have hence modified the abstract as follows, “Aerosol particles in marine atmosphere have been shown to significantly affect cloud formation, atmospheric optical properties, and climate change. However, high temporally and spatially resolved atmospheric measurements over sea are currently sparse, limiting our understanding of aerosol properties in marine atmosphere. In this study, a ship-based cruise campaign was conducted over northern South China Sea (SCS) region during summertime 2018. Chemical composition of non-refractory PM_{10} (NR- PM_{10}), particle number size distribution (PNSD) and size-resolved cloud condensation nuclei (CCN) activity were measured by a time-of-flight aerosol chemical speciation monitor (ToF-ACSM), and the combination of a cloud condensation nuclei counter (CCNc) and a

scanning mobility particle sizer (SMPS), respectively. Overall, aerosol particles exhibited a unimodal distribution centering at 60~80 nm and chemical composition of the NR-PM₁ was dominated by sulfate (~46%) which likely originated from anthropogenic emissions rather than dimethyl sulfide (DMS) oxidation. Two polluted episodes were respectively observed at the beginning (P1) and at the end (P2) of the campaign and both were characterized by high particle number concentrations (N_{CN}) which originated respectively from local emissions and from emissions in inland China via long range transport as shown by back trajectory analysis. The concentrations of trace gases (i.e., O₃, CO, NO_x) and particles (N_{CN} and N_{CCN} at ss=0.34%) were elevated during P2 and decrease with the offshore distance, further suggesting important impacts of anthropogenic emissions from the inland Pearl River Delta (PRD) region on the northern SCS. Two relatively clean periods (C1 and C2) prior to and after tropical storm Bebinca were classified due to substantial removal of pollutants by strong winds and rainfalls accompanying with the storm. During C1 and C2 periods, the air was affected by air masses from southwest and from Indo-China Peninsula, respectively. Chemical composition measurements showed an increase of organic mass fraction during P2 compared to C2; however, no obviously different κ values were obtained from the CCNc measurements, implying that the air masses carried pollutants from local sources during long range transport. We report an average value of about 0.4 for aerosol hygroscopicity parameter κ which falls within the literature values (i.e., 0.2-1.0) for urban and remote marine atmosphere. In addition, our results showed that the CCN fraction (N_{CCN}/N_{CN,tot}) and the κ values obtained from the CCNc measurements (ss=0.34%) had no clear correlation either with the offshore distance or with concentrations of the particles. Our study highlights dynamical variations of particle properties and the impact of long range transport from the China continent and Indo-China Peninsula on the northern SCS region during summertime.”

2. For example, the analysis for the different air masses, came across during the cruise, should be developed further more thorough fashion. I would present available ground data either concentrations of emissions from the different region to discuss their characteristics to elucidate how the chemical evolution affects the outflow to evaluate whether the observational result makes sense or not.

Reply:

We thank the reviewer for valuable suggestions on the air masses analysis and ground data for chemical evolution analysis. We admit that currently physical and chemical properties of aerosol particles based on ground measurements (i.e., chemical composition and particle size distribution) are still largely lacking, especially for long-term measurements. In addition, such nearshore ground measurements and cruise-based measurements are very also scarce, making it hard to evaluate detailed chemical processes for aerosol particles over the SCS region. Besides, we focus on the CCN activity rather than chemical process of aerosol particles over the northern SCS in this study. Based on the above reasons, we analyzed the MODIS fire spots to discuss potential impacts of biomass burning on the air masses which might affect our measurements as shown in Fig. 7 (please refer to answer #5). In addition, we also discuss the contribution of anthropogenic emission to sulfate over the South China Sea based on the MERRA-2 data as shown in Fig. S2. (please refer to answer #3).

3. For example discussion about the presence of sulfate over the South China Sea (line numbers between 269 to 271) can certainly go further by discussing upper end DMS emission rates and whether the assumption can account the observed SO₂.

Reply:

We thank the reviewer for valuable suggestions on sulfate formation. Possible sources of sulfate include ship emissions, DMS oxidation, and transport from inland etc. The oxidation of DMS leads to formation of sulfur dioxide and methanesulfonic acid (MSA) both of which can be further oxidized to produce non-sea-salt (NSS) sulfate in marine atmosphere. Oxidation of SO₂ from ship emissions or inland transport can also be a major source of NSS sulfate (Savoie et al., 2002). As an intermediate between DMS and sulfate, MSA in principle can be detected by ToF-ACSM, although resolution of the instrument is low. We are currently working on MSA identification and quantification from this cruise measurement. Preliminary results show that the fraction of sulfate from DMS oxidation is far below that from ship emissions. An early study showed that anthropogenic sulfate accounted for about 81-97% of NSS sulfate over China Sea (Guo et al., 1996). A ratio of 15-655 NSS sulfate to MSA in PM_{2.5} was reported in the Northern South China Sea (Zhang et al., 2007), much higher than that (18-20) in the remote marine (Savoie et al., 2002). Here we employed the Modern-Era Retrospective analysis for

Research and Applications, Version 2 (MERRA-2) to analyze the distribution of ratio of sulfate to MSA at 925 hPa during the measurement period. The results were shown in Fig. S2 and the ratio ranged from 100 to 10000 over the SCS, much higher than that in the remote Pacific Ocean (1-50). In addition, it also increases with latitude, indicating that the anthropogenic emission is the major source of the total sulfate in the Northern SCS region.

To be clarified, we have added several sentences to discuss the origin of sulfate on p13-14 (L257-270) in the revision, “The oxidation of DMS leads to formation of sulfur dioxide and methansulfonic acid (MSA) both of which can be further oxidized to produce non-sea-salt (NSS) sulfate in marine atmosphere. Oxidation of SO₂ from ship emissions or inland transport can also be a major source of NSS sulfate (Savoie et al., 2002). As an intermediate between DMS and sulfate, MSA in principle can be detected by ToF-ACSM, although resolution of the instrument is low. Preliminary results show that the fraction of sulfate from DMS oxidation is far below that from ship emissions. An early study showed that anthropogenic sulfate accounted for about 81-97% of NSS sulfate over China Sea (Gao et al., 1996). A ratio of 15-655 NSS sulfate to MSA in PM_{2.5} was reported in the northern South China Sea (Zhang et al., 2007), much higher than that (18-20) in the remote marine (Savoie et al., 2002). Here we employed the Modern-Era Retrospective analysis for Research and Applications, Version 2 (MERRA-2) to analyze the distribution of ratio of sulfate to MSA at 925 hPa during the measurement period (GMAO, 2015). The results were shown in Fig. S2 and the ratio ranged from 100 to 10000 over the SCS, much higher than that in the remote Pacific Ocean (1-50). In addition, it also increases with latitude, indicating that the anthropogenic emission is likely the major source of the total sulfate in the northern SCS region.”

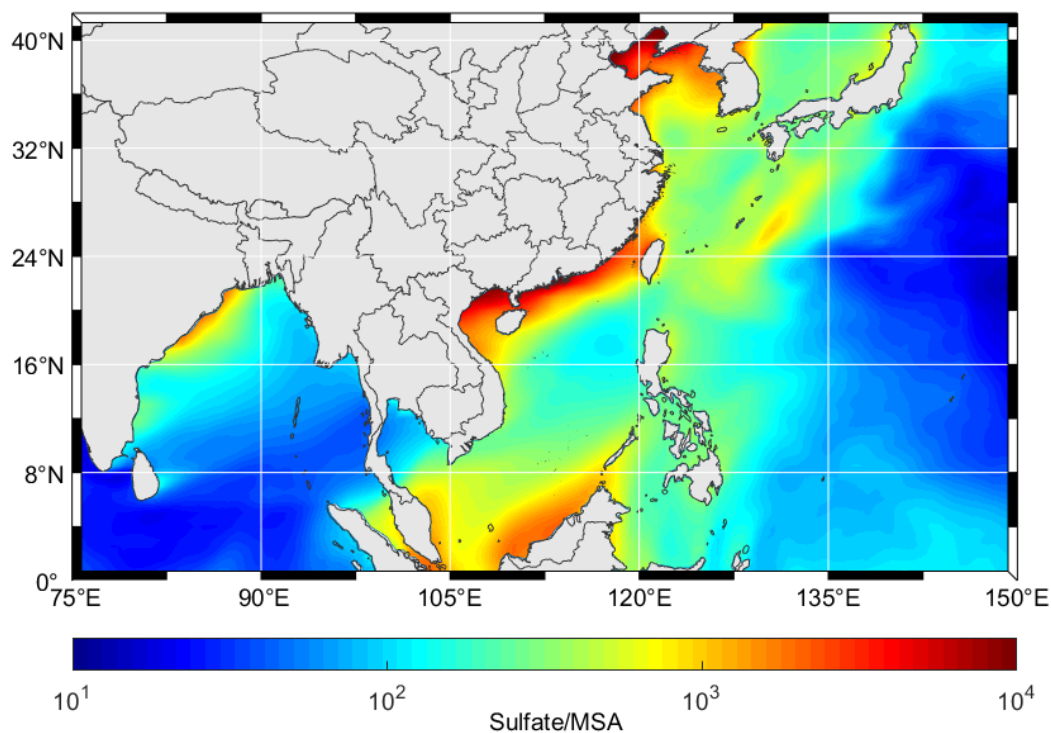


Figure S2. The ratio of sulfate to MSA at 925 hPa from MERRA-2 reanalysis dataset (GMAO, 2015).

4. Another example is in line 342. CO is an obvious long lived tracer for pollution, therefore the correlation of CO with parcels # is not surprising. I would recommend the authors to discuss further more process level aerosol chemistry evolution than these rather one dimensional comparisons of observables.

Reply:

We agree with the reviewer that CO is a long lived tracer for pollution and its correlation with particles might be expected. However, in a recent study, CO was used as a wildfire tracer to study the impact on aerosol properties in the marine atmosphere and it was found that CO concentration had a strong correlation with non-volatile particle concentration ($R^2=0.70$) (Zheng et al., 2020). Here we used CO as a tracer for biomass burning or anthropogenic emissions. We found that CO is not always correlated with particles, for example, it is indeed correlated with particles during the second half of the cruise while is not correlated at all during the first half. Hence CO can be used as a useful tracer for source identification. In this paper, we focus on the effects of pollution on CCN activity. Detailed source apportionment and chemical processes will be the focus of our next paper.

We have added several sentences on p17 (L338-344) in the revision, “The variation of SO₂ concentration was independent of N_{CN}, suggesting that SO₂ did not share the same source with particles. The CO concentration is positively correlated with N_{CN} during the second half of the cruise, while no obvious correlation is observed during the first half, implying that sources of particles could be different during the two periods. The correlation during the second half of the cruise indicates that the particles might share the same source with CO which was attributed to biomass burning or anthropogenic emissions.”

5. It is even more troubling by attributing biomass burning sources as presented in lines between 403 to 405. I would recommend to take full advantage of your wealthy dataset and back trajectory analysis to solidly argue the origin of the observed air mass of biomass burning.

Reply:

The K can be a tracer of biomass burning and sea salt. However, the vaporizer of ACSM and AMS can produce a large amount of K⁺, which will interfere the ambient K signal. To our knowledge, there could be a large uncertainty of the K concentration measured by ACSM. The levoglucosan can also be the tracer of biomass burning. Nevertheless, the mass resolution of our ACSM is too low to distinguish levoglucosan from other species. Currently, there are no direct evidences indicating the impact of biomass burning. We analyzed fire detection data during the measurements from MODIS in combination with back trajectories during C2 which clearly show that the air parcels pass through the fire region. We have modified Fig. 7 and added a discussion on p20 (L407-410), “The backward trajectories during C2 pass through the burning regions in Southeast Asia (e.g., Viet Nam, Laos, Cambodia etc.), also supporting this conjecture. However, more solid evidences are needed since the observation of biomass burning tracers (such as K and levoglucosan) is missing in this campaign.”

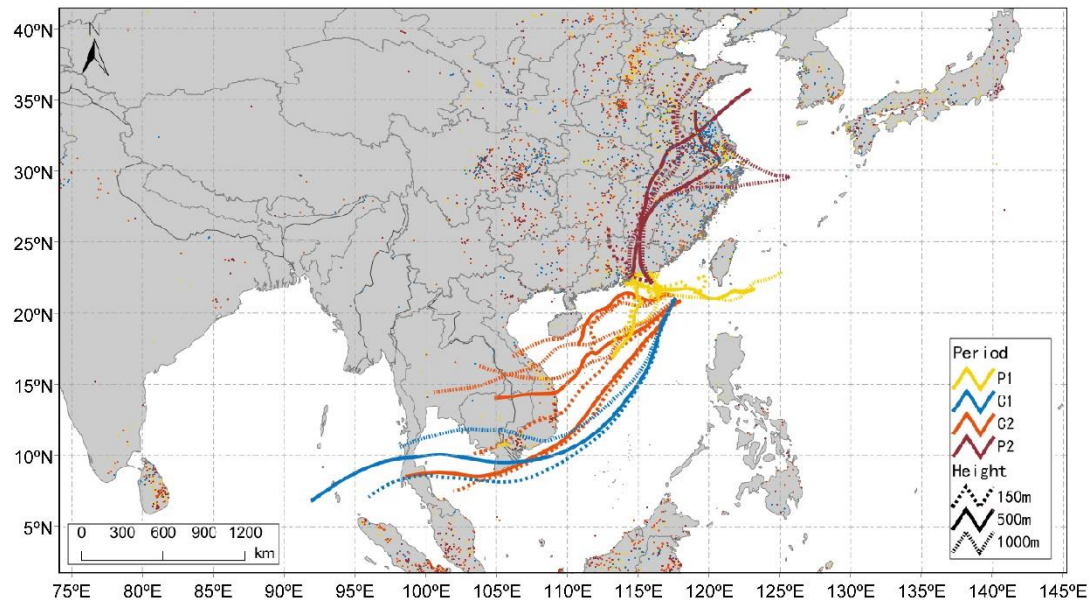


Figure 7. The 72 h backward trajectories arriving at the location of the vessel with three heights (150 m, 500 m, and 1000 m) during P1, C1, C2, and P2, respectively. The dots represent the fire spots detected by MODIS.

Reference:

Global Modeling and Assimilation Office (GMAO) (2015), MERRA-2 inst3_3d_aer_Nv: 3d,3-Hourly,Instantaneous,Model-Level,Assimilation,Aerosol Mixing Ratio V5.12.4, Greenbelt, MD, USA, Goddard Earth Sciences Data and Information Services Center (GES DISC), Accessed: 8, 2018, 10.5067/LTVB4GPCOTK2

Geng, X., Mo, Y., Li, J., Zhong, G., Tang, J., Jiang, H., Ding, X., Malik, R. N., and Zhang, G.: Source apportionment of water-soluble brown carbon in aerosols over the northern South China Sea: Influence from land outflow, SOA formation and marine emission, *Atmospheric Environment*, 229, 117484, <https://doi.org/10.1016/j.atmosenv.2020.117484>, 2020.

Huang, S., Wu, Z., Poulain, L., van Pinxteren, M., Merkel, M., Assmann, D., Herrmann, H., and Wiedensohler, A.: Source apportionment of the organic aerosol over the Atlantic Ocean from 53°N to 53°S: significant contributions from marine emissions and long-range transport, *Atmos. Chem. Phys.*, 18, 18043-18062, 10.5194/acp-18-18043-2018, 2018.

Zheng, G., Sedlacek, A. J., Aiken, A. C., Feng, Y., Watson, T. B., Raveh-Rubin, S., Uin, J., Lewis, E. R., and Wang, J.: Long-range transported North American wildfire aerosols observed in marine boundary layer of eastern North Atlantic, *Environ. Int.*, 139, 105680, <https://doi.org/10.1016/j.envint.2020.105680>, 2020.

1 **Effects of continental emissions on Cloud Condensation**
2 **Nuclei (CCN) activity in northern South China Sea during**
3 **summertime 2018**

4 Mingfu Cai^{1,2,4}, Baoling Liang¹, Qibin Sun¹, Shengzhen Zhou¹, Xiaoyang Chen⁶, Bin Yuan⁴,
5 Min Shao⁴, Haobo Tan^{2*}, and Jun Zhao^{1,3,5*}

6 ¹ School of Atmospheric Sciences, Guangdong Province Key Laboratory for Climate Change and Natural
7 Disaster Studies, and Institute of Earth Climate and Environment System, Sun Yat-sen University,
8 Guangzhou, Guangdong 510275, China

9 ² Institute of Tropical and Marine Meteorology/Guangdong Provincial Key Laboratory of Regional
10 Numerical Weather Prediction, CMA, Guangzhou 510640, China

11 ³ Southern Marine Science and Engineering Guangdong Laboratory (Zhuhai), Zhuhai, Guangdong
12 519082, China

13 ⁴ Institute for Environmental and Climate Research, Jinan University, Guangzhou, Guangdong 511443,
14 China

15 ⁵ Guangdong Provincial Observation and Research Station for Climate Environment and Air Quality
16 Change in the Pearl River Estuary, Guangzhou, Guangdong 510275, China

17 ⁶ Department of Civil and Environmental Engineering, Northeastern University, Boston, MA 02115,
18 USA

19 **Corresponding authors: Jun Zhao (zhaojun23@mail.sysu.edu.cn) and Haobo Tan (hbtan@gd121.cn)*

20

21 **Abstract.** Aerosol particles in marine atmosphere have been shown to significantly affect cloud
22 formation, atmospheric optical properties, and climate change. However, high temporally and spatially
23 resolved atmospheric measurements over sea are currently sparse, limiting our understanding of aerosol
24 properties in marine atmosphere. In this study, a ship-based cruise campaign was conducted over northern
25 South China Sea (SCS) region during summertime 2018. Chemical composition of non-refractory PM₁
26 (NR-PM₁), particle number size distribution (PNSD) and size-resolved cloud condensation nuclei (CCN)

27 activity were measured by a time-of-flight aerosol chemical speciation monitor (ToF-ACSM), and the
28 combination of a cloud condensation nuclei counter (CCNc) and a scanning mobility particle sizer
29 (SMPS), respectively. Overall, aerosol particles exhibited a unimodal distribution centering at 60~80 nm
30 and chemical composition of the NR-PM₁ was dominated by sulfate (~46%) which likely originated from
31 anthropogenic emissions rather than dimethyl sulfide (DMS) oxidation. Two polluted episodes were
32 respectively observed at the beginning (P1) and at the end (P2) of the campaign and both were
33 characterized by high particle number concentrations (N_{CN}) which originated respectively from local
34 emissions and from emissions in inland China via long range transport as shown by back trajectory
35 analysis. The concentrations of trace gases (i.e., O₃, CO, NO_x) and particles (N_{CN} and N_{CCN} at ss=0.34%)
36 were elevated during P2 and decrease with the offshore distance, further suggesting important impacts
37 of anthropogenic emissions from the inland Pearl River Delta (PRD) region on the northern SCS. Two
38 relatively clean periods (C1 and C2) prior to and after tropical storm Bebinca were classified due to
39 substantial removal of pollutants by strong winds and rainfalls accompanying with the storm. During C1
40 and C2 periods, the air was affected by air masses from southwest and from Indo-China Peninsula,
41 respectively. Chemical composition measurements showed an increase of organic mass fraction during
42 P2 compared to C2; however, no obviously different κ values were obtained from the CCNc
43 measurements, implying that the air masses carried pollutants from local sources during long range
44 transport. We report an average value of about 0.4 for aerosol hygroscopicity parameter κ which falls
45 within the literature values (i.e., 0.2-1.0) for urban and remote marine atmosphere. In addition, our results
46 showed that the CCN fraction (N_{CCN}/N_{CN,tot}) and the κ values obtained from the CCNc measurements
47 (ss=0.34%) had no clear correlation either with the offshore distance or with concentrations of the
48 particles. Our study highlights dynamical variations of particle properties and the impact of long range

49 transport from the China continent and Indo-China Peninsula on the northern SCS region during
50 summertime.

51 **1 Introduction**

52 Aerosol particles directly affect global radiation balance by scattering and absorbing solar radiation.
53 Meanwhile, they can alter cloud microphysics, lifetime, and albedo, indirectly affecting heat transfer
54 through atmosphere (Stocker, 2013). However, high uncertainties still exist on their contributions to the
55 climatic impact, partly owing to our limited knowledge on spatial and temporal distribution of aerosol
56 particles and their properties in various environments. Thus, it is essential to conduct field measurements
57 under different environments to obtain chemical and physical properties of particles, including chemical
58 composition, particle number size distribution (PNSD), and cloud condensation nuclei (CCN) activity,
59 in order to better understand the radiation forcing induced by aerosol particles.

60 The CCN activity describes how particles grow into cloud droplets and further affect cloud
61 development. Whether particles can be activated as CCN is determined by their chemical composition,
62 hygroscopicity, size, and ambient supersaturation (ss). Generally, the CCN activity can be described by
63 Köhler theory based on the water activity in solution, surface tension, molecular weight of water,
64 temperature, and diameter of the particle (Köhler, 1936). Alternatively, the hygroscopicity parameter κ
65 proposed by Petters and Kreidenweis (2007) can be used to characterize the CCN activity. Aerosol
66 hygroscopicity describes the ability of particles to grow by absorbing moisture in ambient environments.
67 The κ values can be measured in subsaturation ($RH < 100\%$) condition by the hygroscopicity-tandem
68 differential mobility analyzer (HTDMA) measurements or in supersaturation ($RH > 100\%$) by the cloud
69 condensation nuclei counter (CCNc) measurements.

70 Field measurements for the CCN activity have been conducted primarily in terrestrial environments
71 (e.g., urban cities, forested areas, and remote countryside areas) (Rose et al., 2010; Wang et al., 2010;
72 Cerully et al., 2011; Pierce et al., 2012; Hong et al., 2014; Cai et al., 2018). Cerully et al. (2011) reported

73 κ values ranging from 0.1 to 0.4 in forest during the 2007 EUCAARI campaign and concluded that the
74 κ values obtained from the HTDMA measurements were generally 30% lower than those from the CCNc
75 measurements. Wang et al. (2010) showed that the mixing state of particles was important in predicting
76 the CCN number concentration (N_{CCN}). Cai et al. (2018) found that the CCN activity increased by
77 decreasing the surface tension through increase of organic fractions in particles based on the
78 measurements of the CCN activity, hygroscopicity, and chemical composition in the Pearl River Delta
79 (PRD) region. Progresses on the aforementioned field measurements conducted in the continental
80 environments have substantially improved our understanding of the influence of aerosols in global
81 radiation forcing and precipitation under the terrestrial environments.

82 Aerosol particles in the marine atmosphere, on the other hand, have been well known to significantly
83 affect cloud development, atmospheric optical properties, and climate change (Johnson et al., 2004;
84 Ackerman et al., 2004; Mulcahy et al., 2008). Fewer field measurements were conducted in the oceanic
85 atmosphere than those in land, leading to less characterization of marine aerosol particles. Remote
86 sensing and ship-based cruise methods are two typical approaches employed to measure aerosol
87 properties in marine environments (Durkee et al., 1986; Kim et al., 2009; Lehahn et al., 2010; Huang et
88 al., 2018). Compared to ship-based measurements, remote sensing covers spatially a larger area and
89 temporally a longer period which are essential in the characterization of marine aerosols. For example,
90 Reid et al. (2013) employed remote sensing to describe long range transport patterns in the Southeast
91 Asia. The aerosol size information was compared between the retrievals from Moderate Resolution
92 Imaging Spectroradiometer (MODIS) and the measurements from ground-based radiometers such as
93 Aerosol Robotic Network (AERONET) over ocean (Kleidman et al., 2005). However, extensive cloud
94 coverages over oceanic region can significantly affect the quality and availability of satellite

95 measurements. **Meanwhile**, dry bias or clear-sky bias also challenge satellite measurements for obtaining
96 accurate data (John et al., 2011; Reid et al., 2013; Choi and Ghim, 2017). Moreover, remote sensing using
97 satellite sensors is limited in providing high time resolution (i.e., minutes), high spatial resolution (i.e.,
98 within tens of meters in dimension) data and specific particle properties (i.e., hygroscopicity and
99 chemical composition). Although ship-based measurements are limited in spatial coverage, they can
100 provide higher spatial and temporal resolution for obtaining comprehensive physical and chemical
101 properties of gas and aerosol particles. Huang et al. (2018) measured chemical composition of particles
102 with a high-resolution time-of-flight aerosol mass spectrometer (HR-ToF-AMS) over the Atlantic Ocean
103 aboard a campaign ship and found that about 19% of organics originated from continental long-range
104 transport. Kim et al. (2009) found that particle size distribution varied in a dynamic range, depending on
105 the meteorological conditions over the Yellow Sea and the East China Sea. Atwood et al. (2017) showed
106 that biomass burning, anthropogenic pollution from continent and ship emissions would affect the remote
107 South China Sea during the southwestern monsoon (SWM) season. However, few ship-based campaigns
108 are available in the literature on measurements of atmospheric composition including gases and aerosol
109 particles, especially in several important China sea regions (e.g., SCS).

110 The air over northern SCS is affected by anthropogenic pollution from the adjacent Pearl River
111 Delta region, China inner continent, and Indo-China Peninsula (Zhang et al., 2018). Furthermore, as one
112 of the most important and busy trading regions in China, the PRD and the northern SCS are subjected to
113 severe air pollution due to emissions from heavy loadings of cargo ships and fishing vessels (Lv et al.,
114 2018). Special weather patterns are dominant in the SCS during summertime which are characterized by
115 SWM and occasionally affected by typhoons. Typically, typhoon brings heavy precipitation and strong
116 wind to this region, which helps to remove air pollutants. However, on one hand, it has been found that

117 downdrafts prior to a typhoon usually affect negatively atmospheric diffusion, leading to the
118 accumulation of the air pollutants in the region (Feng et al., 2007). On the other hand, marine background
119 particles and emissions from Indo-China Peninsula are brought into this region through SWM. As a result,
120 the physical and chemical properties of marine aerosol particles vary dynamically which can be
121 distinguished from those of continental particles. Differences (i.e., physical and chemical properties, life
122 cycle) between the two types of aerosol particles reflect different transport pathways and source origins
123 which are not well known. In addition, lack of understanding on aerosol characteristics will inevitably
124 hinder our ability to evaluate the impacts of aerosol particles on global radiation forcing and atmospheric
125 processes. Thus, ship-based field measurements are urgently needed in this region in order to understand
126 the CCN activity, chemical composition, particle size distribution, and their relationships with
127 continental and marine air masses.

128 In this study, we report results from a recent ship-based cruise measurement in the northern SCS
129 during summertime 2018. During the campaign, size-resolved CCN activity, chemical composition, and
130 particle number size distribution were measured by a CCNc, a time-of-flight aerosol chemical speciation
131 monitor (ToF-ACSM) and a scanning mobility particle sizer (SMPS), respectively. Temporal and spatial
132 distributions of the aerosol chemical and physical properties and impact of different air masses on the
133 properties were investigated. Our results provide valuable knowledge on the effects of long range
134 transport and on the atmospheric processes in the SCS.

135

136 2 Methodology

137 2.1 Ship-based campaign

138 The cruise campaign is a routine comprehensive exercise organized by Sun Yat-sen University
139 (SYSU) during summertime 2018 (6th to 27th August) including a variety of multidisciplinary sciences
140 (i.e., atmosphere, ocean, chemistry, geology, and biology). The round-trip journey started and ended at
141 Huizhou port (22°43' N, 114°36' E), which is about 140 km from Guangzhou, traveling towards northern
142 SCS with an area between 19°37' N to 22°43' N and 113°44' E to 118°12' E. The ship track includes two
143 routes during which the vessel was anchored near the port due to tropical storm Bebinca as its track was
144 shown in Fig. 1a, along with the complete, color-coded ship track. The first route started 7th August from
145 the port and arrived northeast of Dongsha Islands (20°45' N 118°12' E) on 10th August 2018, and then
146 returned to anchor near the port during the typhoon period (11th to 15th August). The second route left the
147 port on 15th August toward Hong Kong and arrived at its south in the afternoon (18:00 local time, LT).
148 The vessel then headed southeast for about 42 hours on 18th August and turned toward Dongsha Islands.
149 It anchored at several sites around this sea area and then returned on 24th August following a similar
150 pathway as the first route to Huizhou port on 27th August.

151 A commercial vessel with a capacity of 8000 ton was employed for the routine summer
152 measurement campaign whose schematic diagram was shown in Fig. 1b. An air conditioned (T=298K)
153 sea container of about 30 m² housed all the instruments which was listed in Table 1 and was placed in
154 the front deck of the vessel. Trace gases, including O₃, SO₂, CO, NO_x (NO and NO₂), were measured by
155 gas analyzers (model T400U, T100U, T300, and T200U, Teledyne API Inc., USA, respectively). Detailed
156 descriptions of the major instruments used in the campaign could be found in the following subsection.

157 The aerosol sampling port with a PM_{2.5} cyclone inlet was made of a 5 m long 3/8" o.d. stainless-steel
158 tube which extended outside of the container with an inclination angle of 45° to the deck. The inlet is
159 about 2.5 m above the deck and 1.5 m away from the container. All aerosol sampling flows firstly passed
160 through a Nafion dryer (model MD-700, Perma Pure Inc., USA) to reach a relative humidity (RH) lower
161 than 30%. The gas sample inlet made of a 2 m long 1/4" o.d. Teflon tube with a similar inclination angle,
162 also extended outside of the container.

163

164 **2.2 Origins of air masses by HYSPLIT**

165 The HYbrid Single-Particle Lagrangian Integrated Trajectory (HYSPLIT) model developed by
166 National Oceanic and Atmospheric Administration (NOAA) was used to investigate trajectories of air
167 movement for identification of source origins which might affect the northern SCS region during the
168 campaign. The model calculated the 72 hours back trajectories of air masses at 6 hours intervals arriving
169 at the campaign vessel. The arrival height of the trajectories was set to be 150 m, 500 m, and 1000 m
170 above the ground level, a reasonable representative of the air masses. The Global Data Assimilation
171 System (GDAS) 1°× 1° meteorological data was employed to drive the HYSPLIT.

172

173 **2.3 Measurements**

174 **2.3.1 Size-resolved cloud condensation nuclei activity**

175 The size-resolved CCN activity was measured with combination of a homemade scanning mobility
176 particle sizer system and a cloud condensation nuclei counter (model CCNc-200, DMT Inc., USA). The

177 homemade SMPS system consisted of a differential mobility analyzer (DMA, model 3081L, TSI., Inc.)
178 and a condensation particle counter (CPC, model 3787, TSI Inc.). The CCNc-200 has two parallel cloud
179 columns (column A and B) which measure the CCN concentrations (N_{CCN}) at two specific ss at the same
180 time. Only the N_{CCN} measured by column A was discussed in this study. During the measurements, the
181 SMPS system was operated in a scanning mode. The sample particles after the Nafion dryer were firstly
182 neutralized by a X-ray neutralizer (model 3088, TSI., Inc., USA) and were subsequently classified by the
183 DMA. The selected particles were split into the CPC for measurements of total particle number
184 concentration (with a flow rate of 0.6 LPM) and the CCNc for measurements of the CCN number
185 concentration at a specific supersaturation (with a flow rate of 0.5 LPM). The SMPS and the CCNc
186 system were set to measure particle number size distribution and size-resolved CCN number
187 concentration at a mobility size range of 10-400 nm. The supersaturation of the CCNc was set to be
188 0.18%, 0.34%, and 0.59%. Before the measurements, the CCNc-200 was calibrated with ammonium
189 sulfate ($(NH_4)_2SO_4$) particles at three ss (0.18%, 0.34%, and 0.59%), detailed description of the
190 calibration could be found in Cai et al. (2018). The SMPS system was also calibrated with standard
191 polystyrene latex spheres (PSL, with a size of 20 nm, 50 nm, and 200 nm) prior to the campaign.

192

193 **2.3.2 Aerosol chemical composition**

194 An Aerodyne time-of-flight aerosol chemical speciation monitor was deployed to measure bulk non-
195 refractory PM_{10} chemical composition during the campaign. The ToF-ACSM can provide mass
196 concentration of sulfate, nitrate, ammonium, chloride, and organics, except non-refractory components
197 such as sea salt, black carbon, and crustal species. Detailed description of ToF-ACSM can be found in
198 Fröhlich et al. (2013) and only a brief introduction relevant to this work was given here. During the

199 campaign, the measurement cycle of the ToF-ACSM was set to be about 10 min and the mass resolving
200 power was about 160. The sample flow dried by the Nafion dryer entered an automatic three-way valve,
201 of which one way was directly connected to the lens system and the other way was connected to a filter
202 before entering the aerodynamic lens. By switching the automatic valve periodically, the instrument can
203 measure the total signal without a filter and the background signal with a filter, thus the net signal
204 representing the chemical composition of the aerosol particles can be obtained. The aerodynamic lens
205 system removes particles larger than 1 μm (at aerodynamic diameter, D_{VA}) and has a relative low
206 transmission for small particles ($D_{VA} < 50$ nm). Monodisperse pure ammonium nitrate (NH_4NO_3) and
207 ammonium sulfate ($(\text{NH}_4)_2\text{SO}_4$) particles generated by a homemade atomizer and then selected by a
208 DMA (about 300 nm in diameter) were used to calibrate the relative ionization efficiency (RIE) value of
209 NH_4 (RIE_{NH_4}) and SO_4 (RIE_{SO_4}) at the beginning and at the end of the campaign.

210

211 2.4 Data processing of CCN activation

212 The size-resolved N_{CN} and N_{CCN} measured by the SMPS and CCNc-200 system was used to
213 calculate the activation ratio (AR), which was defined as the ratio of N_{CCN} to N_{CN} at each size bin. The
214 size-resolved ARs were inverted based on the method described by Moore et al. (2010). The AR spectrum
215 was then fitted using a three-parameter fit:

$$216 \quad \frac{N_{CCN}}{N_{CN}} = \frac{B}{1 + \left(\frac{D_p}{D_{50}}\right)^C}, \quad (1)$$

217 where D_p represents dry particle diameter (nm), B, C and D_{50} are the three fitting parameters which
218 represent the asymptote, the slope, and the inflection point of the sigmoid, respectively (Moore et al.,
219 2010). The D_{50} is called the critical diameter, where 50% of the particles are activated at a specific ss.

220 A hygroscopicity parameter κ which represents the CCN activity was calculated from the critical

221 saturation ratio (S_c) and D_{50} from the following equation (Petters and Kreidenweis, 2007):

$$222 \quad \kappa = \frac{4A^3}{27D_{50}^3(\ln S_c)^2}, \quad A = \frac{4\sigma_{s/a}M_w}{RT\rho_w}, \quad (2)$$

223 where ρ_w is density of pure water (about 997.04 kg m⁻³ at 298.15K), M_w is molecular weight of water
224 (0.018 kg mol⁻¹), $\sigma_{s/a}$ is surface tension of the solution/air interface which is assumed to be value of pure
225 water ($\sigma_{s/a}$ = 0.0728 N m⁻¹ at 298.15K), R is the universal gas constant (8.314 J mol⁻¹ K⁻¹), T is
226 thermodynamic temperature in Kelvin (298.15K), and D_{50} is the critical diameter (in meter).

227

228 **3 Results and Discussion**

229 **3.1 Overview**

230 Figure 2 shows number size distribution (a), mass concentration and fraction (b and c), number
231 concentration of CCN (d), and hygroscopicity parameter (e) measured by different instruments during
232 the campaign. The particle sizes were predominantly larger than 10 nm, implying that no new particle
233 formation events were observed during the campaign. Furthermore, the distribution exhibited mainly
234 unimodal characteristics which peaked at a size range of about 60-80 nm. The average number
235 concentration was about 3400 cm⁻³, which was in general lower than that in inland PRD region (Cai et
236 al., 2017) and slightly lower than the ship measurement (4335 cm⁻³) over the East China Sea (Kim et al.,
237 2009). However, two relative polluted periods were classified with high particle number concentrations
238 at the beginning (6th-8th August, defined as P1 with a particle size peaking at about 80 nm) and at the end
239 (25th-26th August, defined as P2 peaking at about 100 nm) of the campaign. In contrast, two relatively
240 clean periods were identified in between (9th-10th August, defined as C1 and 19th-21st August, defined as
241 C2).

242 Temporal profile of the mass concentration (Fig. 2a) measured by ToF-ACSM was consistent with
243 that of PNSD, which showed the highest concentration on 25th August. The total measured mass
244 concentration of NR-PM₁ varied dramatically from 0.92 to 85.08 $\mu\text{g m}^{-3}$, with a median of 7.97 $\mu\text{g m}^{-3}$.
245 Mass concentrations of PM_{2.5} were reported over the same region during Cruise I (27.6 $\mu\text{g m}^{-3}$) and
246 Cruise II (10.10 $\mu\text{g m}^{-3}$) in Zhang et al. (2007). The mass concentration in our measurements was higher
247 than that in clean marine atmosphere (from 0.27 to 1.05 $\mu\text{g m}^{-3}$) reported at the coastal station, Ireland
248 (Ovadnevaite et al., 2014) and the atmosphere over the Atlantic Ocean (Huang et al., 2018). Mass
249 concentration of SO₄²⁻ varied from 0.35 to 33.20 $\mu\text{g m}^{-3}$, with a median of 3.66 $\mu\text{g m}^{-3}$, which falls in a
250 range of previous measurement in Dongsha Islands (1.3 to 5.5 $\mu\text{g m}^{-3}$, Chuang et al., 2013). The average
251 mass fraction of NR-PM₁ during the campaign was dominated by sulfate (46%), followed by organics
252 (35%), ammonium (14%), nitrate (3%), and chloride (2%), which was similar to the measurement over
253 the Atlantic Ocean (Huang et al., 2018). The chemical composition over northern SCS was quite different
254 from that at the urban site which was dominated by organics largely from anthropogenic sources (Cai et
255 al., 2017). A higher mass fraction of sulfate in the marine atmosphere may probably be attributed to
256 anthropogenic emissions (such as nearby ship emissions) rather than oxidation of dimethyl sulfide (DMS)
257 emitted from the ocean. The oxidation of DMS leads to formation of sulfur dioxide and methansulfonic
258 acid (MSA) both of which can be further oxidized to produce non-sea-salt (NSS) sulfate in marine
259 atmosphere. Oxidation of SO₂ from ship emissions or inland transport can also be a major source of NSS
260 sulfate (Savoie et al., 2002). As an intermediate between DMS and sulfate, MSA in principle can be
261 detected by ToF-ACSM, although resolution of the instrument is low. Preliminary results show that the
262 fraction of sulfate from DMS oxidation is far below that from ship emissions. An early study showed
263 that anthropogenic sulfate accounted for about 81-97% of NSS sulfate over China Sea (Gao et al., 1996).

264 A ratio of 15-655 NSS sulfate to MSA in PM_{2.5} was reported in the northern South China Sea (Zhang et
265 al., 2007), much higher than that (18-20) in the remote marine (Savoie et al., 2002). Here we employed
266 the Modern-Era Retrospective analysis for Research and Applications, Version 2 (MERRA-2) to analyze
267 the distribution of ratio of sulfate to MSA at 925 hPa during the measurement period (GMAO, 2015).
268 The results were shown in Fig. S2 and the ratio ranged from 100 to 10000 over the SCS, much higher
269 than that in the remote Pacific Ocean (1-50). In addition, it also increases with latitude, indicating that
270 the anthropogenic emission is likely the major source of the total sulfate in the northern SCS region.

271 The number concentrations of CCN (N_{CCN} at $ss=0.18\%$, 0.34% , and 0.59%) and total particles (N_{CN})
272 were shown in Fig. 2d. The N_{CN} values during the two polluted periods (P1 and P2) were significantly
273 higher than the average N_{CN} (3463 cm^{-3}) over the whole campaign period and those from other marine
274 measurements (Cai et al., 2017; Kim et al., 2009). This average value falls between the smoke type (2280
275 cm^{-3}) and the port type (4890 cm^{-3}) measured over the remote South China Sea (Atwood et al., 2017).
276 Note that since the abnormally spiked signals which were probably caused by emissions of the nearby
277 ships or the ship itself were removed in the data processes, the high N_{CN} values during those episodes
278 were likely attributed to regional pollution or long range transport from continents. For consistency, we
279 removed spikes likely associated with smoking, emissions from the ship itself and other adjacent ships
280 and cooking from further data analysis, including either abrupt high number concentrations of particles
281 (measured by SMPS), organics (measured by ToF-ACSM), and NO_x (measured by the NO_x monitor)
282 (Detailed criteria can be referred to descriptions and Fig. S1 in supplementary). In general, the N_{CCN}
283 values at the three supersaturations increased with increase of the N_{CN} . The average value of N_{CCN} (1544
284 cm^{-3} , $ss=0.34\%$) was similar with the simulated value ($1000\text{-}2000\text{ cm}^{-3}$, $ss=0.4\%$), suggesting the model
285 simulation could satisfactorily predict the N_{CCN} in this region (Yu and Luo, 2009). Although the N_{CCN}

286 and N_{CN} were relatively higher in P1 and P2 than the average value, they remained overall low during
287 the campaign compared to those from the inland PRD sites. The N_{CCN} values in P1 were lower than those
288 in P2 with similar values of N_{CN} in both P1 and P2, suggesting a lower activation fraction in P1 than in
289 P2, which could be attributed to relatively high fractions of smaller particles and a lower hygroscopicity
290 in P1. As discussed above, particles peaked at a smaller size in P1, leading to fewer particles larger than
291 D_{50} . The time series of the κ values calculated using Eq. 2 show that the aerosol hygroscopicity was lower
292 at the beginning of the campaign, leading to a lower CCN activity in P1. The measurements could be
293 affected by local fresh emissions with lower hygroscopic particles in urban since the ship was anchored
294 near Huizhou port and Hong Kong during P1, similar to lower hygroscopicity for urban particles
295 previously measured by Cai et al. (2017). Furthermore, low particle hygroscopicity was found from 11th
296 August to 15th August when the ship was sheltered at the port from the tropical storm Bebinca.

297 Aerosol hygroscopicity, an important parameter affecting CCN activity, can vary largely in its
298 values under different environments due to a variety of particle sources (Adam et al., 2012; Liu et al.,
299 2014; Hong et al., 2014; Wu et al., 2013; Cai et al., 2017). **Comparison of the hygroscopicity parameter**
300 **κ obtained from this study, urban Guangzhou, remote marine Okinawa, remote South China Sea, and**
301 **mountain Goldlauer was shown in Fig. 3.** The κ_{median} values obtained from this study (around 0.4) fall
302 between those at the continental sites (Guangzhou and Goldlauer) and remote marine measurement
303 (remote South China Sea and Okinawa) and are barely dependent on particle sizes whose pattern is quite
304 similar to those in Okinawa. Moreover, a κ value was respectively reported to be in a range of 0.22-0.65
305 measured by CCNc over the remote South China Sea and in a range of 0.30-0.56 measured by HTDMA
306 over the coast of central California during a flight campaign (Atwood et al., 2017; Hersey et al., 2009).
307 In addition, high hygroscopicity values (0.56-1.04) measured by HTDMA were also reported over the

308 Pacific and Southern Oceans (Berg et al., 1998). In contrast to maritime environments (i.e., SCS and
309 Okinawa), the κ_{median} values in Guangzhou (0.21-0.31) are much lower and increase obviously with
310 particle sizes. The low hygroscopicity for small particles in Guangzhou was attributed to local emissions
311 from traffic and industry (Cai et al., 2017). The cruise in this campaign is in an offshore region where
312 the air is affected by anthropogenic emissions from the adjacent inland PRD region, leading to medium
313 values of aerosol hygroscopicity between urban and marine background regions.

314

315 **3.2 Temporal and spatial distributions**

316 As discussed above, the air over the offshore northern SCS is affected by local emissions from
317 inland PRD regions. The shoreline along Huizhou port is roughly 45° inclined to the latitude (from South
318 to North) and it is reasonable to assume that the concentrations of the air pollutants originating from local
319 emissions are generally dependent on the distance offshore which can be roughly represented by the
320 latitude in this study. Hence in this section, the temporal and spatial concentration distributions of air
321 pollutants (particles and gases) were presented with latitude and the dates were color-coded, representing
322 from the beginning (dark blue) to the end (dark red) of the cruise (Fig. 4). The concentrations of trace
323 gases (O_3 , CO, and NO_x), N_{CN} , and N_{CCN} ($ss=0.34\%$) were higher during the late half than during early
324 half of the campaign, while SO_2 concentration varied in an opposite way, suggesting that the sources of
325 the air pollutants or the air masses were different at the beginning and at the ending of the campaign. In
326 particular, the aforementioned quantities increased substantially with latitude (the higher the latitude the
327 closer to the shore) from 19th to 26th August, indicating that the air masses from inland China could affect
328 the northern SCS region during this period. However, the $N_{\text{CCN}}/N_{\text{CN,tot}}$ and κ values ($ss=0.34\%$) showed

329 almost no pattern (Figs. 4g and 4h), except that the $N_{CCN}/N_{CN,tot}$ values were both high (about 0.8) at the
330 beginning and at the end of the cruise. The $N_{CCN}/N_{CN,tot}$ was defined as the ratio of number concentration
331 of cloud condensation nuclei and total aerosol particles at a specific ss. The κ values were observed to be
332 relatively low when the vessel located at a latitude of about 22°N corresponding to 6th and 26th August,
333 suggesting that the air was affected by local fresh emissions which increased the organic content of the
334 particles. Interestingly, a higher value on 26th August than on 6th August was clearly shown (Fig. 4g) due
335 probably to larger averaged particle sizes on 26th August (about 110 nm) which were more easily
336 activated than smaller particles on 6th August (about 60-90 nm).

337 To further investigate the effects of local emissions on aerosol particles over northern SCS, the
338 correlations of SO₂, CO, NO_x concentration, N_{CCN} , $N_{CCN}/N_{CN,tot}$, κ with N_{CN} were explored (Fig. 5). **The**
339 **variation of SO₂ concentration was independent of N_{CN} , suggesting that SO₂ did not share the same source**
340 **with particles. The CO concentration is positively correlated with N_{CN} during the second half of the cruise,**
341 **while no obvious correlation is observed during the first half, implying that sources of particles could be**
342 **different during the two periods. The correlation during the second half of the cruise indicates that the**
343 **particles might share the same source with CO which was attributed to biomass burning or anthropogenic**
344 **emissions.** An excellent correlation between NO_x concentration and N_{CN} was shown in all ranges of
345 particle number concentrations, implying that the aerosol particles might originate from the same source
346 as NO_x which was likely attributed to traffic and industry in the continental PRD region. The N_{CCN} was
347 observed to follow two distinct trends for the first and second half of the cruise which show in general a
348 higher activation efficiency during the second half of the campaign, especially when N_{CN} is greater than
349 about 7000 cm⁻³, further validated by a much higher $N_{CCN}/N_{CN,tot}$ ratio against N_{CN} as shown in Fig. 5e.
350 As discussed in the previous paragraph, distinct κ values were seen at the very beginning and at the end

351 of the campaign, suggesting that the properties and sources of the particles could be different as will be
352 further discussed in the case study below.

353

354 **3.3 Case Study**

355 In section 3.1, we classified four periods (all in August) based upon particle number concentration,
356 corresponding to P1 (6th to 8th), C1 (9th to 10th), C2 (19th to 21st), and P2 (25th to 26th) as shown in Fig. 6.
357 During the two clean periods (C1, before Bebinca; C2, after Bebinca), the vessel travelled around
358 northeast of Dongsha islands where the particle number concentrations remained relatively low which
359 were not affected by the continental emissions from the PRD region. However, high number
360 concentrations of particles were observed during P1 when the vessel was close to the shore where the air
361 was substantially affected by local emissions from either Hongkong or Huizhou. During the last two days
362 in P2, even higher particle number concentrations were observed, suggesting that the pollutants might
363 originate from inland continent via long range transport.

364 We performed HYSPLIT to investigate the source origins of the air pollutants according to
365 movement of air masses during the campaign (Fig. 7). The backward trajectories during P1 showed that
366 the air masses were mainly from east and south and when arriving at the location of the vessel, the air
367 masses were stagnant on the shore, suggesting that the pollutants might originate from local emissions.
368 Interestingly, particle number concentrations were low during 11th to 15th August when the vessel was
369 sheltered from Bebinca, due probably to the arrival of the typhoon which caused high wind speeds and
370 brought rainfall in the northern SCS, resulting in removal of air pollutants in Huizhou and in Hong Kong.
371 The air masses over northern SCS originated from southwest (C1) or from Indo-China Peninsula (C2)
372 due to summer monsoon during the two clean periods (Fig. 7). The air masses moved northerly during

373 P2 and brought high concentrations of particles from inland China to PRD region, and then further to the
374 northern SCS (Fig. 7).

375 Chemical speciation by ToF-ACSM showed that the mass fractions of aerosol composition were
376 substantially different during C1, C2, and P2, except for nitrate whose fraction remain almost constant
377 among the above three periods (Fig. 8). Note that the mass fraction during P1 was not available for
378 comparison due to instrumental failure. Even the mass fractions during the two clean periods were
379 distinctly different, in particular, those of organics (26% for C1 vs 40% for C2), ammonium (19% for C1
380 vs 12% for C2), and chloride (7% for C1 vs 2% for C2), although the particle composition was dominated
381 by sulfate which was almost equal in mass fraction (44% for C1 vs 42% for C2). The mass fraction
382 during C1 was dominated by sulfate, followed by organics, ammonium which was similar to that in
383 remote marine region (Cai et al., 2017). The mass fraction of sulfate in the NR-PM₁ during C1 and C2
384 was also similar to the previous study (44% and 43% in PM_{2.5} for Cruise I and II, respectively) over the
385 northern SCS (Zhang et al., 2007). Although the mass fraction was still dominated by sulfate, a
386 substantially increasing fraction of organic (increase of 26% for C1 to 40% for C2) was observed. This
387 increase in organic fraction was likely attributed to the air masses passing through Indo-China Peninsula
388 which brought significant local sources. In contrast to the clean periods, the mass fraction in the NR-PM₁
389 during P2 was dominated by organics (47%), followed by sulfate (33%) and ammonium (13%), similar
390 to that in urban areas (Huang et al., 2014), indicating that air masses from the north could bring
391 continental particles in inland China to the northern SCS.

392 The particle number size distribution (PNSD) was measured by the custom-made SMPS which was
393 described in the methodology section. The average particle number concentrations during P1 and P2
394 (9239 and 10088 cm⁻³ respectively) were much higher than those during the clean periods (1826 and

395 1683 cm^{-3} for C1 and C2 respectively). In addition, the PNSD during the pollution periods was
396 characterized by an obvious accumulation mode that was attributed to secondary aerosols (Fig. 9), while
397 the one during the clean periods has a smaller and a less obvious accumulation mode and a more obvious
398 Aitken mode which was more related to marine background particles (Cai et al., 2017; Atwood et al.,
399 2017; Kim et al., 2009). The median diameters and concentration of the accumulation mode during C1
400 and C2 was similar to those previously reported in South China Sea (Reid et al., 2015). Note that the
401 fitted nucleation modes for both clean and pollution periods were barely seen due to the obviously low
402 concentrations of particles in this mode. The lognormal median diameters for the Aitken mode (70.4 nm)
403 and the accumulation mode (165.7 nm) during P2 were respectively larger than those (48.6 nm and 143.1
404 nm) during P1, implying more aging processes and particle growth in the long range transport from the
405 inland continent. Furthermore, a wider accumulation mode during C2 than during C1 was observed,
406 implying more complex sources for larger size particles which could probably be attributed to biomass
407 burning or anthropogenic activities across Indo-China Peninsula. **The backward trajectories during C2**
408 **pass through the burning regions in Southeast Asia (e.g., Viet Nam, Laos, Cambodia etc.), also supporting**
409 **this conjecture. However, more solid evidences are needed since the observation of biomass burning**
410 **tracers (such as K and levoglucosan) is missing in this campaign.**

411 The CCN activity parameters (average N_{CCN} , D_{50} , and $N_{\text{CCN}}/N_{\text{CN,tot}}$ at $ss=0.18\%$, 0.34% , and 0.59%)
412 during each period were summarized in Table 2. The N_{CCN} ($ss=0.34\%$) during P1 and P2 were 3969 and
413 7139 cm^{-3} , much higher than the simulated annual mean values in northern SCS region (1000-2000
414 cm^{-3} , $ss=0.4\%$, Yu and Luo, 2009). It implies that the continental emissions could have significant impact
415 on the CCN concentration over this region. Although the mass fractions of chemical composition for C1,
416 C2, and P2 were quite different among those periods, no significant differences of the hygroscopicity

417 parameter κ values were seen, indicating particles with a size range of 30-120 nm were less affected by
418 long range transport from Indo-China Peninsula or inland China continent. The calculated median κ
419 values based on the measured D_{50} ranged from 0.32 to 0.41 and no significant differences in diameters
420 and periods were observed (Fig. S3), suggesting that the high mass fractions of organics during C2 might
421 be distributed in larger particle sizes (Fig. 8). The D_{50} values during P2 were smaller at all supersaturation
422 ratios, suggesting higher hygroscopicity and CCN activity during this period. In addition, the $N_{CCN}/N_{CN,tot}$
423 and N_{CCN} during P2 was larger than during P1, owing to a larger number fraction of accumulation mode
424 and a higher hygroscopicity. Meanwhile, the median κ values fell in a range of 0.12-0.19 during P1,
425 significantly lower than those during three other periods but similar to the values measured in urban cities
426 (Tan et al., 2013; Jiang et al., 2016; Cai et al., 2018). Such lower values of hygroscopicity were probably
427 contributed from local emissions originating from inland urban cities or heavy duty ships. More cruise
428 campaigns are hence needed to identify the source origins of marine aerosols over the SCS region.

429 The mixing state and heterogeneity of particles can affect the steepness of the activation curves (Cai
430 et al., 2018). A steeper curve indicates that particles intend to be internally mixed and have a higher
431 similarity in hygroscopicity. The average activation curves at 0.18% ss during the P1, C1, C2 and P2
432 periods are shown in Fig. S4. The parameter C (in Eq. 1) can be used to present the steepness of activation
433 curve. A small C value indicates a steep activation curve. The C values during P1, C1, C2 and P2 periods
434 were -8.5, -14.3, -13.7 and -10.6, respectively. The smooth curve and the largest C value during P1
435 suggest that particles had a higher degree of external mixing and higher heterogeneity, owing to the local
436 fresh emissions. The C values during C1 and C2 periods were close and smaller than those in pollution
437 periods, implying particles during clean periods were more aged and tend to be more internally mixed.
438 The backward trajectories show that the air masses during clean periods were less affected by fresh

439 emissions. The activation curve during P2 period was smoother than C1 and C2 but steeper than P1,
440 indicating that the particles during this period could be a mixture of aged particles from China inland and
441 fresh particles from onshore emissions.

442

443 **4 Conclusions**

444 As an annual routine exercise for SCS expedition during summertime, the 2018 cruise campaign
445 organized by Sun Yat-sen University is a comprehensive and interdisciplinary field measurement
446 involving atmosphere, ocean, geology, biology, and chemistry etc. The measurement includes stationary
447 and navigating observations based on compromise among multiple disciplines. For atmospheric
448 measurements, several key scientific questions are emerging to be addressed over SCS region, including
449 sources of air pollutants (gases and particles) in marine atmosphere, impacts of biomass burning from
450 southeastern Asia and summer monsoon on atmospheric chemistry and physics in SCS region. In this
451 study, the CCN activity, chemical composition, and particle number size distribution over northern SCS
452 were measured using several onboard instruments including a ToF-ACSM, a CCNc, a SMPS, several
453 monitors for trace gases (i.e., SO₂, NO_x, CO, and O₃). On one hand, lower concentrations of key trace
454 gas pollutants and particle number or mass were observed in atmosphere of SCS than those in urban
455 areas in PRD region, consistent with previously reported values for background marine atmosphere.
456 Overall, chemical composition of NR-PM₁ was dominated by sulfate (46%) and the PNSD showed
457 unimodal distribution centering at about 60-80 nm and the hygroscopicity κ values being higher than
458 those in urban areas. On the other hand, characteristics of air pollutants (e.g., concentrations, physical
459 and chemical properties) show substantially variations during summer monsoon season, depending on

460 source origins. Characteristics similar to continental aerosols were shown when air masses originate from
461 inland China continent or Indo-China peninsula possibly via long range transport, leading to increase of
462 organic fraction in chemical composition and decrease of hygroscopicity which might be attributed to
463 picking up locally emitted and fresh pollutants during transport. Furthermore, low hygroscopicity κ
464 values were shown when the air was affected by local fresh emissions and in this case the number
465 concentration of particles increased with decrease of offshore distance. In addition, concentrations of
466 both NO_x and CCN concentrations were well correlated with the total concentration of particles.
467 Interestingly, a tropical storm Bebinca was caught in the middle of the campaign, resulting in two
468 relatively clean periods (C1 and C2). These clean periods were likely attributed to strong wind and
469 rainfalls brought by the storm which could obviously blow away or wash out pollutants in northern SCS
470 region.

471 Our results suggest that aerosol properties and trace gases concentration over northern SCS is
472 complex and substantially variable. The median hygroscopicity κ values of the particles in northern SCS
473 were measured to be about 0.4, in the range of between those in the remote northwestern Pacific Ocean
474 and those in urban PRD region, implying that particles in northern SCS could be a mixture of marine
475 background and anthropogenic particles from continents (e.g., Indo-China peninsula and inland China
476 continent). Concentrations of aerosol particles and trace gases exhibit complex temporal and spatial
477 distribution. Concentrations of trace gases (i.e., O_3 , CO, and NO_x except SO_2), particles (i.e., N_{CN} and
478 N_{CCN}) were higher at the beginning (pollution episode: P1) than at the end (pollution episode: P2) of the
479 campaign, implying different source origins for the two periods. At the beginning of the campaign, the
480 air was likely affected by local fresh emissions from Huizhou, leading to increase of concentrations of
481 both measured trace gases (except SO_2) and particles with decrease of offshore distance. Meanwhile,

482 concentration of NO_x had a good correlation with the N_{CN} , suggesting they might originate from the
483 same sources. Similarly, at the end of the campaign, concentrations of both measured trace gases (except
484 SO_2) and particles also increased with decrease of offshore distance, while because of more larger
485 particles, higher fractions of particles were activated at the end than at the beginning of the campaign.
486 We attributed the source origin during this period to inland China content via long range transport with
487 additional local fresh pollutants during transport process, leading to barely clear patterns for both
488 $N_{\text{CCN}}/N_{\text{CN,tot}}$ and D_{50} at all applied ss ($ss=0.18, 0.34, \text{ and } 0.59\%$). Furthermore, our results indicate that
489 biomass burning from southeastern Asia may have important impacts on chemical composition and
490 properties of aerosol particles over northern SCS, in particular, leading to increase of organic mass
491 fractions and decrease of hygroscopicity κ values and hence affecting CCN activity in the region. Our
492 study highlights the necessity for performing more intensive ship-based atmospheric measurements in
493 order to better understand marine aerosols and air pollution in SCS region.

494

495 *Data availability.* Data from the ship-based cruise measurements are available upon request (Jun Zhao
496 via zhaojun23@mail.sysu.edu.cn).

497

498 *Supplement.* The supplement related to this article is available online at xxx.

499

500 *Author contributions.* **MC**, **JZ**, and **HT** designed the research. **MC** and **BL** performed the ship-based
501 cruise measurements. **XC** performed sulfate/MSA analysis. **MC**, **JZ**, **HT**, **BL**, and **QS** analyzed the data.

502 **MC**, **JZ**, and **HT** wrote the paper with contributions from all co-authors.

503

504 *Competing interests.* The authors declare that they have no conflict of interest.

505

506 *Acknowledgements.* We acknowledges support from National Key Project of MOST (2017YFC0209502,
507 2016YFC0201901, 2016YFC2003305), National Natural Science Foundation of China (NSFC)
508 (91644225, 21577177, 41775117), Science and Technology Innovation Committee of Guangzhou
509 (201803030010), the “111 plan” Project of China (Grant B17049), Scientific and Technological
510 Innovation Team Project of Guangzhou Joint Research Center of Atmospheric Sciences, China
511 Meteorological Administration (Grant No.201704). Additional support from the crew of the vessel and
512 from Southern Marine Science and Engineering Guangdong Laboratory (Zhuhai) is greatly
513 acknowledged.

514 **References**

515 Ackerman, A. S., Kirkpatrick, M. P., Stevens, D. E., and Toon, O. B.: The impact of humidity above
516 stratiform clouds on indirect aerosol climate forcing, *Nature*, 432, 1014, 2004.

517 Adam, M., Putaud, J. P., Martins dos Santos, S., Dell'Acqua, A., and Gruening, C.: Aerosol
518 hygroscopicity at a regional background site (Ispra) in Northern Italy, *Atmos. Chem. Phys.*, 12, 5703-
519 5717, 2012.

520 Atwood, S. A., Reid, J. S., Kreidenweis, S. M., Blake, D. R., Jonsson, H. H., Lagrosas, N. D., Xian, P.,
521 Reid, E. A., Sessions, W. R., and Simpas, J. B.: Size-resolved aerosol and cloud condensation nuclei
522 (CCN) properties in the remote marine South China Sea – Part 1: Observations and source
523 classification, *Atmos. Chem. Phys.*, 17, 1105-1123, 2017.

524 Berg, O. H., Swietlicki, E., and Krejci, R.: Hygroscopic growth of aerosol particles in the marine
525 boundary layer over the Pacific and Southern Oceans during the First Aerosol Characterization
526 Experiment (ACE 1), *J. Geophys. Res.-Atmos.*, 103, 16535-16545, 1998.

527 Cai, M., Tan, H., Chan, C. K., Mochida, M., Hatakeyama, S., Kondo, Y., Schurman, M. I., Xu, H., Li, F.,
528 and Shimada, K.: Comparison of Aerosol Hygroscopicity, Volatility, and Chemical Composition
529 between a Suburban Site in the Pearl River Delta Region and a Marine Site in Okinawa, *Aerosol Air
530 Qual. Res.*, 17, 3194-3208, 2017.

531 Cai, M., Tan, H., Chan, C. K., Qin, Y., Xu, H., Li, F., Schurman, M. I., Li, L., and Zhao, J.: The size
532 resolved cloud condensation nuclei (CCN) activity and its prediction based on aerosol hygroscopicity
533 and composition in the Pearl Delta River (PRD) Region during wintertime 2014, *Atmos. Chem. Phys.*,
534 18, 16419-16437, 2018.

535 Cerully, K., Raatikainen, T., Lance, S., Tkacik, D., Tiitta, P., Petäjä, T., Ehn, M., Kulmala, M., Worsnop,

536 D., and Laaksonen, A.: Aerosol hygroscopicity and CCN activation kinetics in a boreal forest
537 environment during the 2007 EUCAARI campaign, *Atmos. Chem. Phys.*, 11, 12369-12386, 2011.

538 Choi, Y., and Ghim, Y. S.: Assessment of the clear-sky bias issue using continuous PM10 data from two
539 AERONET sites in Korea, *J. Environ. Sci.*, 53, 151-160, 2017.

540 Chuang, M.-T., Chang, S.-C., Lin, N.-H., Wang, J.-L., Sheu, G.-R., Chang, Y.-J., and Lee, C.-T.: Aerosol
541 chemical properties and related pollutants measured in Dongsha Island in the northern South China
542 Sea during 7-SEAS/Dongsha Experiment, *Atmos. Environ.*, 78, 82-92, 4, 2013.

543 Durkee, P. A., Jensen, D., Hindman, E., and Haar, T.: The relationship between marine aerosol particles
544 and satellite-detected radiance, *J. Geophys. Res.-Atmos.*, 91, 4063-4072, 1986.

545 Feng, Y., Wang, A., Wu, D., and Xu, X.: The influence of tropical cyclone Melor on PM10 concentrations
546 during an aerosol episode over the Pearl River Delta region of China: Numerical modeling versus
547 observational analysis, *Atmos. Environ.*, 41, 4349-4365, 2007.

548 Fröhlich, R., Cubison, M. J., Slowik, J. G., Bukowiecki, N., Prévôt, A. S. H., Baltensperger, U., Schneider,
549 J., Kimmel, J. R., Gonin, M., and Rohner, U.: The ToF-ACSM: a portable aerosol chemical speciation
550 monitor with TOFMS detection, *Atmos. Meas. Tech.*, 6, 3225-3241, 2013.

551 Gao, Y., Arimoto, R., Duce, R. A., Chen, L. Q., Zhou, M. Y., and Gu, D. Y.: Atmospheric non-sea-salt
552 sulfate, nitrate and methanesulfonate over the China Sea, *J. Geophys. Res. Atmos.*, 101, 12601-12611,
553 1996.

554 Global Modeling and Assimilation Office (GMAO) (2015), MERRA-2 inst3_3d_aer_Nv: 3d,3-
555 Hourly,Instantaneous,Model-Level,Assimilation,Aerosol Mixing Ratio V5.12.4, Greenbelt, MD,
556 USA, Goddard Earth Sciences Data and Information Services Center (GES DISC), Accessed: 8,
557 2018, [10.5067/LTVB4GPCOTK2](https://doi.org/10.5067/LTVB4GPCOTK2).

558 Hersey, S., Sorooshian, A., Murphy, S., Flagan, R., and Seinfeld, J.: Aerosol hygroscopicity in the marine
559 atmosphere: A closure study using high-time-resolution, multiple-RH DASH-SP and size-resolved
560 C-ToF-AMS data, *Atmos. Chem. Phys.*, 9, 2543-2554, 2009.

561 Hong, J., Häkkinen, S. A. K., Paramonov, M., Äijälä, M., Hakala, J., Nieminen, T., Mikkilä, J., Prisle, N.
562 L., Kulmala, M., and Riipinen, I.: Hygroscopicity, CCN and volatility properties of submicron
563 atmospheric aerosol in a boreal forest environment during the summer of 2010, *Atmos. Chem. Phys.*,
564 14, 29097-29136, 2014.

565 Huang, R., Zhang, Y., Bozzetti, C., Ho, K.-F., Cao, J.-J., Han, Y., Daellenbach, K. R., Slowik, J. G., Platt,
566 S. M., and Canonaco, F.: High secondary aerosol contribution to particulate pollution during haze
567 events in China, *Nature*, 514, 218, 2014.

568 Huang, S., Wu, Z., Poulain, L., Pinxteren, M. V., Merkel, M., Assmann, D., Herrmann, H., and
569 Wiedensohler, A.: Source apportionment of the submicron organic aerosols over the Atlantic Ocean
570 from 53° N to 53° S using HR-ToF-AMS, *Atmos. Chem. Phys.*, 18, 1-35, 2018.

571 Jiang, R., Tan, H., Tang, L., Cai, M., Yin, Y., Li, F., Liu, L., Xu, H., Chan, P. W., and Deng, X.:
572 Comparison of aerosol hygroscopicity and mixing state between winter and summer seasons in Pearl
573 River Delta region, China, *Atmos. Res.*, 169, 160-170, 2016.

574 John, V. O., Holl, G., Allan, R. P., Buehler, S. A., Parker, D. E., and Soden, B. J.: Clear-sky biases in
575 satellite infrared estimates of upper tropospheric humidity and its trends, *J. Geophys. Res.-Atmos.*,
576 116, D14108, doi:10.1029/2010JD015355, 2011.

577 Johnson, B., Shine, K., and Forster, P.: The semi-direct aerosol effect: Impact of absorbing aerosols on
578 marine stratocumulus, *Q. J. Roy. Meteor. Soc.*, 130, 1407-1422, 2004.

579 Köhler, H.: The nucleus in and the growth of hygroscopic droplets, *T. Faraday Soc.*, 32, 1152-1161, 1936.

580 Kim, J. H., Yum, S. S., Lee, Y. G., and Choi, B. C.: Ship measurements of submicron aerosol size
581 distributions over the Yellow Sea and the East China Sea, *Atmos. Res.*, 93, 700-714, 2009.

582 Kleidman, R. G., O'Neill, N. T., Remer, L. A., Kaufman, Y. J., Eck, T. F., Tanré, D., Dubovik, O., and
583 Holben, B. N.: Comparison of Moderate Resolution Imaging Spectroradiometer (MODIS) and
584 Aerosol Robotic Network (AERONET) remote-sensing retrievals of aerosol fine mode fraction over
585 ocean, *J. Geophys. Res.-Atmos.*, 110, D22205, doi:10.1029/2005JD005760, 2005.

586 Lehahn, Y., Koren, I., Boss, E., Ben-Ami, Y., and Altaratz, O.: Estimating the maritime component of
587 aerosol optical depth and its dependency on surface wind speed using satellite data, *Atmos. Chem.
588 Phys.*, 10, 6711-6720, 2010.

589 Liu, H. J., Zhao, C. S., Nekat, B., Ma, N., Wiedensohler, A., van Pinxteren, D., Spindler, G., Müller, K.,
590 and Herrmann, H.: Aerosol hygroscopicity derived from size-segregated chemical composition and
591 its parameterization in the North China Plain, *Atmos. Chem. Phys.*, 14, 2525-2539, 2014.

592 Lv, Z., Liu, H., Ying, Q., Fu, M., Meng, Z., Wang, Y., Wei, W., Gong, H., and He, K.: Impacts of shipping
593 emissions on PM_{2.5} pollution in China, *Atmos. Chem. Phys.*, 18, 15811–15824, 2018.

594 Moore, R. H., Nenes, A., and Medina, J.: Scanning Mobility CCN Analysis-A Method for Fast
595 Measurements of Size-Resolved CCN Distributions and Activation Kinetics, *Aerosol Sci. Tech.*, 44,
596 861-871, 2010.

597 Mulcahy, J., O'Dowd, C., Jennings, S., and Ceburnis, D.: Significant enhancement of aerosol optical
598 depth in marine air under high wind conditions, *Geophys. Res. Lett.*, 35, L16810,
599 doi:10.1029/2008GL034303, 2008.

600 Ovadnevaite, J., Ceburnis, D., Leinert, S., Dall'Osto, M., Canagaratna, M., O'Doherty, S., Berresheim,
601 H., and O'Dowd, C.: Submicron NE Atlantic marine aerosol chemical composition and abundance:

602 Seasonal trends and air mass categorization, *J. Geophys. Res.-Atmos.*, 119, 11,850-811,863, 2014.

603 Petters, M., and Kreidenweis, S.: A single parameter representation of hygroscopic growth and cloud
604 condensation nucleus activity, *Atmos. Chem. Phys.*, 7, 1961-1971, 2007.

605 Pierce, J., Leaitch, W., Liggio, J., Westervelt, D., Wainwright, C., Abbatt, J., Ahlm, L., Al-Basheer, W.,
606 Cziczo, D., and Hayden, K.: Nucleation and condensational growth to CCN sizes during a sustained
607 pristine biogenic SOA event in a forested mountain valley, *Atmos. Chem. Phys.*, 12, 3147-3163, 2012.

608 Reid, J. S., Hyer, E. J., Johnson, R. S., Holben, B. N., Yokelson, R. J., Zhang, J., Campbell, J. R.,
609 Christopher, S. A., Di Girolamo, L., and Giglio, L.: Observing and understanding the Southeast Asian
610 aerosol system by remote sensing: An initial review and analysis for the Seven Southeast Asian
611 Studies (7SEAS) program, *Atmos. Res.*, 122, 403-468, 2013.

612 Reid, J. S., Lagrosas, N. D., Jonsson, H. H., Reid, E. A., Sessions, W. R., Simpas, J. B., Uy, S. N., Boyd,
613 T., Atwood, S. A., and Blake, D. R.: Observations of the temporal variability in aerosol properties
614 and their relationships to meteorology in the summer monsoonal South China Sea/East Sea: the scale-
615 dependent role of monsoonal flows, the Madden–Julian Oscillation, tropical cyclones, squall lines
616 and cold pools, *Atmos. Chem. Phys.*, 15, 1745-1768, 2015.

617 Rose, D., Nowak, A., Achtert, P., Wiedensohler, A., Hu, M., Shao, M., Zhang, Y., Andreae, M. O., and
618 Pöschl, U.: Cloud condensation nuclei in polluted air and biomass burning smoke near the mega-city
619 Guangzhou, China – Part 1: Size-resolved measurements and implications for the modeling of aerosol
620 particle hygroscopicity and CCN activity, *Atmos. Chem. Phys.*, 10, 3365-3383, 2010.

621 Savoie, D. L., Arimoto, R., Keene, W. C., Prospero, J. M., Duce, R. A., and Galloway, J. N.: Marine
622 biogenic and anthropogenic contributions to non-sea-salt sulfate in the marine boundary layer over
623 the North Atlantic Ocean, *J. Geophys. Res. Atmos.*, 107, AAC 3-1-AAC 3-21, 10.1029/2001JD000970,

624 2002.

625 Stocker, D. Q.: Climate change 2013: The physical science basis, Working Group I Contribution to the
626 Fifth Assessment Report of the Intergovernmental Panel on Climate Change, Summary for
627 Policymakers, IPCC, 2013.

628 Tan, H., Yin, Y., Gu, X., Li, F., Chan, P. W., Xu, H., Deng, X., and Wan, Q.: An observational study of
629 the hygroscopic properties of aerosols over the Pearl River Delta region, *Atmos. Environ.*, 77, 817-
630 826, 2013.

631 Wang, J., Cubison, M., Aiken, A., Jimenez, J., and Collins, D.: The importance of aerosol mixing state
632 and size-resolved composition on CCN concentration and the variation of the importance with
633 atmospheric aging of aerosols, *Atmos. Chem. Phys.*, 10, 7267-7283, 2010.

634 Wu, Z. J., Poulain, L., Henning, S., Dieckmann, K., Birmili, W., Merkel, M., van Pinxteren, D., Spindler,
635 G., Müller, K., Stratmann, F., Herrmann, H., and Wiedensohler, A.: Relating particle hygroscopicity
636 and CCN activity to chemical composition during the HCCT-2010 field campaign, *Atmos. Chem.*
637 *Phys.*, 13, 7983-7996, 2013.

638 Yu, F., and Luo, G.: Simulation of particle size distribution with a global aerosol model: contribution of
639 nucleation to aerosol and CCN number concentrations, *Atmos. Chem. Phys.*, 9, 7691-7710, 2009.

640 Zhang, M., Wang, Y., Ma, Y., Wang, L., Gong, W., and Liu, B.: Spatial distribution and temporal variation
641 of aerosol optical depth and radiative effect in South China and its adjacent area, *Atmos. Environ.*,
642 188, 120-128, 2018.

643 Zhang, X., Zhuang, G., Guo, J., Yin, K., and Zhang, P.: Characterization of aerosol over the Northern
644 South China Sea during two cruises in 2003, *Atmos. Environ.*, 41, 7821-7836, 2007.

645

646

Table 1. Summary of the instruments used in the campaign.

| Instruments | Parameters |
|-------------------------|--|
| ToF-ACSM | NR-PM ₁ |
| SMPS+CCNc | PNSD (9-415 nm), Size-resolved CCN Activation Ratio (at ss=0.18%, 0.34%, and 0.59%) |
| CO Monitor | CO concentration |
| SO ₂ Monitor | SO ₂ concentration |
| O ₃ Monitor | O ₃ concentration |
| NO _x Monitor | NO _x , NO, NO ₂ concentration |

647

648

649 **Table 2.** Summary of average N_{CCN} , D_{50} , and $N_{CCN}/N_{CN,tot}$ at 0.18%, 0.34%, and 0.59% ss during P1,
 650 C1, C2, and P2.

| Period | ss | 0.18% | 0.34% | 0.59% |
|--------|---------------------------------|-------|-------|-------|
| P1 | N_{CCN} (# cm^{-3}) | 1825 | 3969 | 7198 |
| | D_{50} (nm) | 132 | 96 | 65 |
| | $N_{CCN}/N_{CN,tot}$ | 0.19 | 0.34 | 0.49 |
| C1 | N_{CCN} (# cm^{-3}) | 566 | 978 | 1330 |
| | D_{50} (nm) | 105 | 67 | 49 |
| | $N_{CCN}/N_{CN,tot}$ | 0.31 | 0.54 | 0.71 |
| C2 | N_{CCN} (# cm^{-3}) | 536 | 844 | 1183 |
| | D_{50} (nm) | 108 | 68 | 48 |
| | $N_{CCN}/N_{CN,tot}$ | 0.32 | 0.55 | 0.73 |
| P2 | N_{CCN} (# cm^{-3}) | 4969 | 7140 | 8679 |
| | D_{50} (nm) | 101 | 65 | 49 |
| | $N_{CCN}/N_{CN,tot}$ | 0.49 | 0.74 | 0.85 |

651

652

653 FIGURE CAPTIONS

654 Figure 1. Ship track and tropical storm Bebinca track during the campaign (a), and schematic diagram of
655 the vessel showing the location of the sea container which housed the onboard instruments during the
656 campaign (b).

657 Figure 2. Temporal profiles of the measured particle number size distribution (a), mass concentration (b)
658 and mass fraction (c) of chemical composition, N_{CCN} and N_{CN} (d) and the daily averaged κ values with
659 the upper and lower error bars (e). No data were shown between 6th and 8th August due to the instrumental
660 failure of the TOF-ACSM.

661 Figure 3. The median and interquartile κ values measured over South China Sea, at urban Guangzhou
662 site, at marine background Okinawa site, and the mean and standard deviation κ values measured over
663 remote South China Sea and at mountain Goldlauer site. The κ values over South China Sea were
664 obtained from CCNc measurements (ss=0.18%, 0.34%, and 0.59%, in blue). The κ values in urban
665 Guangzhou were obtained from CCNc (ss=0.1%, 0.2%, 0.4%, and 0.7%, in orange) and HTDMA
666 measurements (in purple). The κ values in marine region Okinawa were obtained from HTDMA
667 measurements (in green). The κ values in remote South China Sea were obtained from CCNc (ss=0.14%
668 and 0.38%, in orange). The κ values in mountain Goldlauer site were obtained from CCNc (ss=0.07%,
669 0.10%, 0.19% and 0.38%, in black).

670 Figure 4. Concentrations of SO₂ (a), O₃ (b), CO(c), NO_x (d), N_{CN} (e), N_{CCN} (f), $N_{CCN}/N_{CN,tot}$ at 0.34% ss
671 (g), and κ at 0.34% ss (h) as a function of latitude. The data points were color-coded according to date.

672 Figure 5. Correlations of SO₂(a), CO(b), NO_x (c), N_{CCN} (d), AR at 0.34% ss (e), and κ at 0.34% ss (f)
673 with N_{CN} . The data were plotted according to color-coded dates.

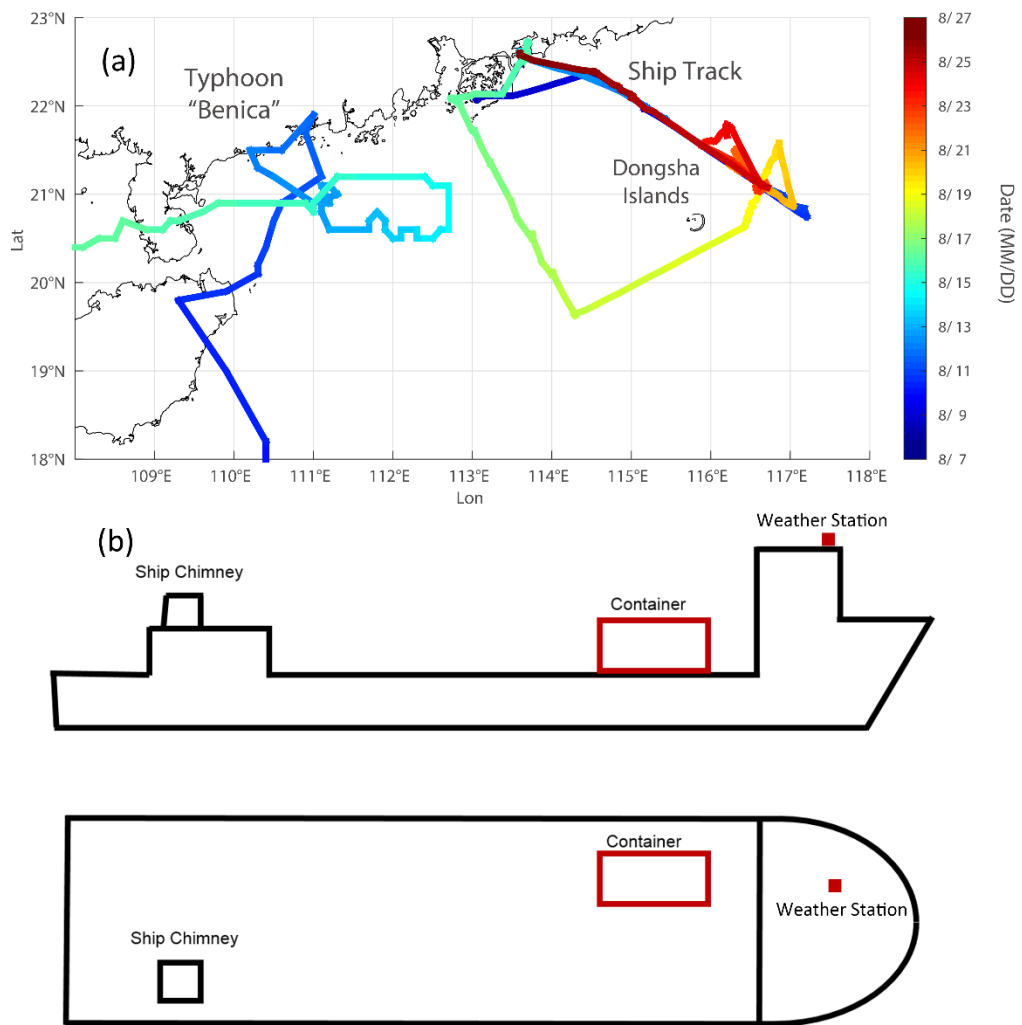
674 Figure 6. The ship track during P1, C1, C2 and P2 periods.

675 Figure 7. The 72 h backward trajectories arriving at the location of the vessel with three heights (150 m,
676 500 m, and 1000 m) during P1, C1, C2, and P2, respectively. The dots represent the fire spots detected
677 by MODIS.

678 Figure 8. The average mass fraction of NR-PM₁ composition during the C1, C2 and P2 periods.

679 Figure 9. The average and standard deviation (shaded area) PNSD, along with trimodal lognormal fitted
680 modes (dash color lines). The average N_{CN} during each period and the median size of each lognormal fit
681 were shown.

682

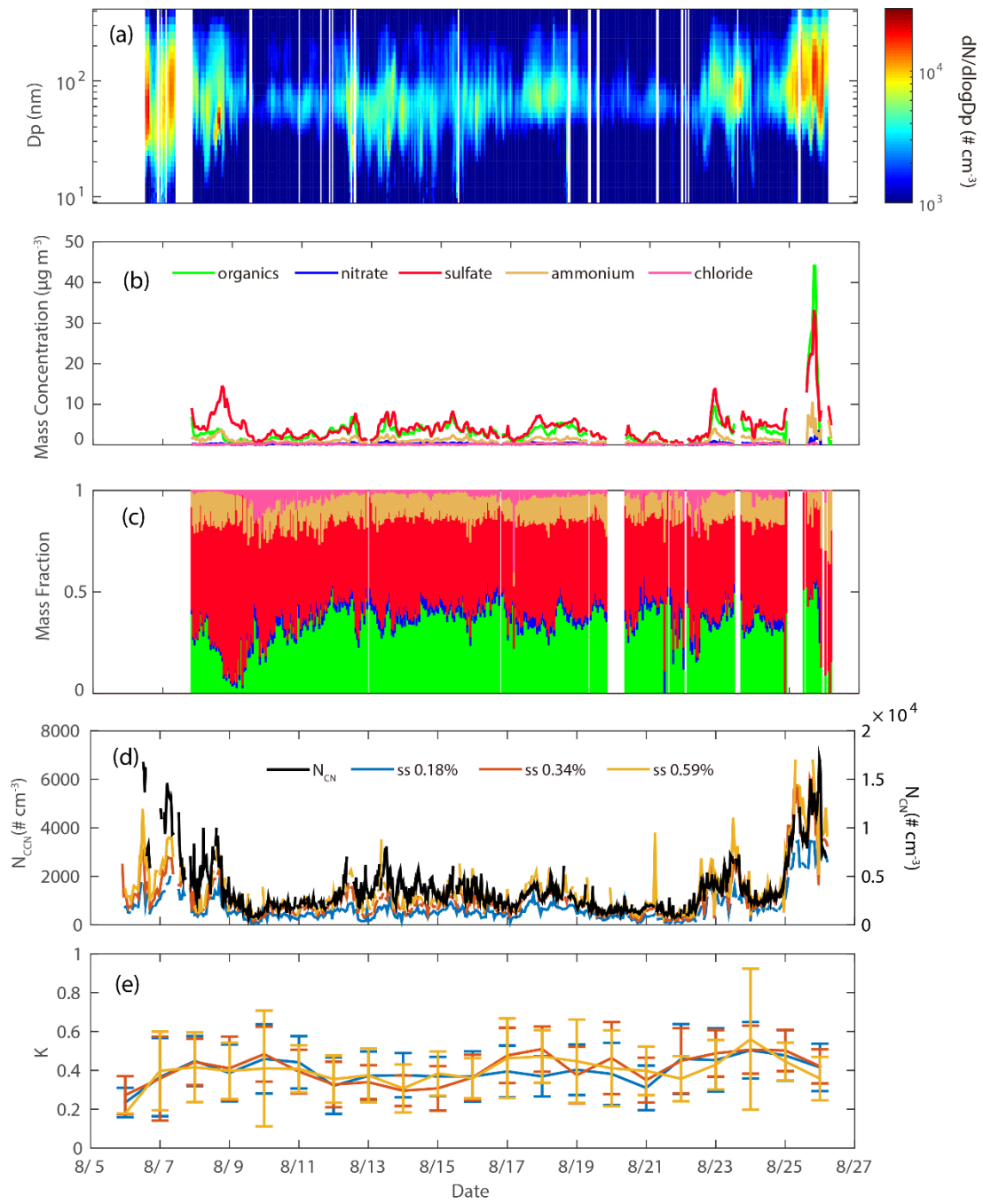


683

684 Fig. 1.

685

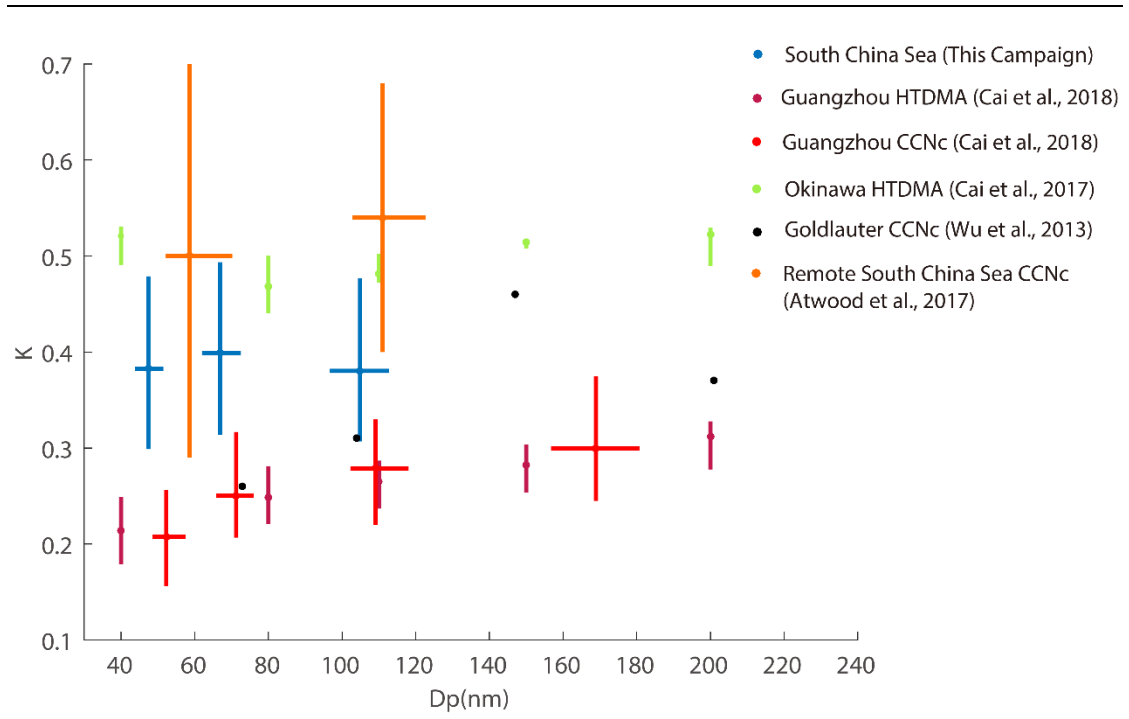
686



687

688 Fig. 2.

689

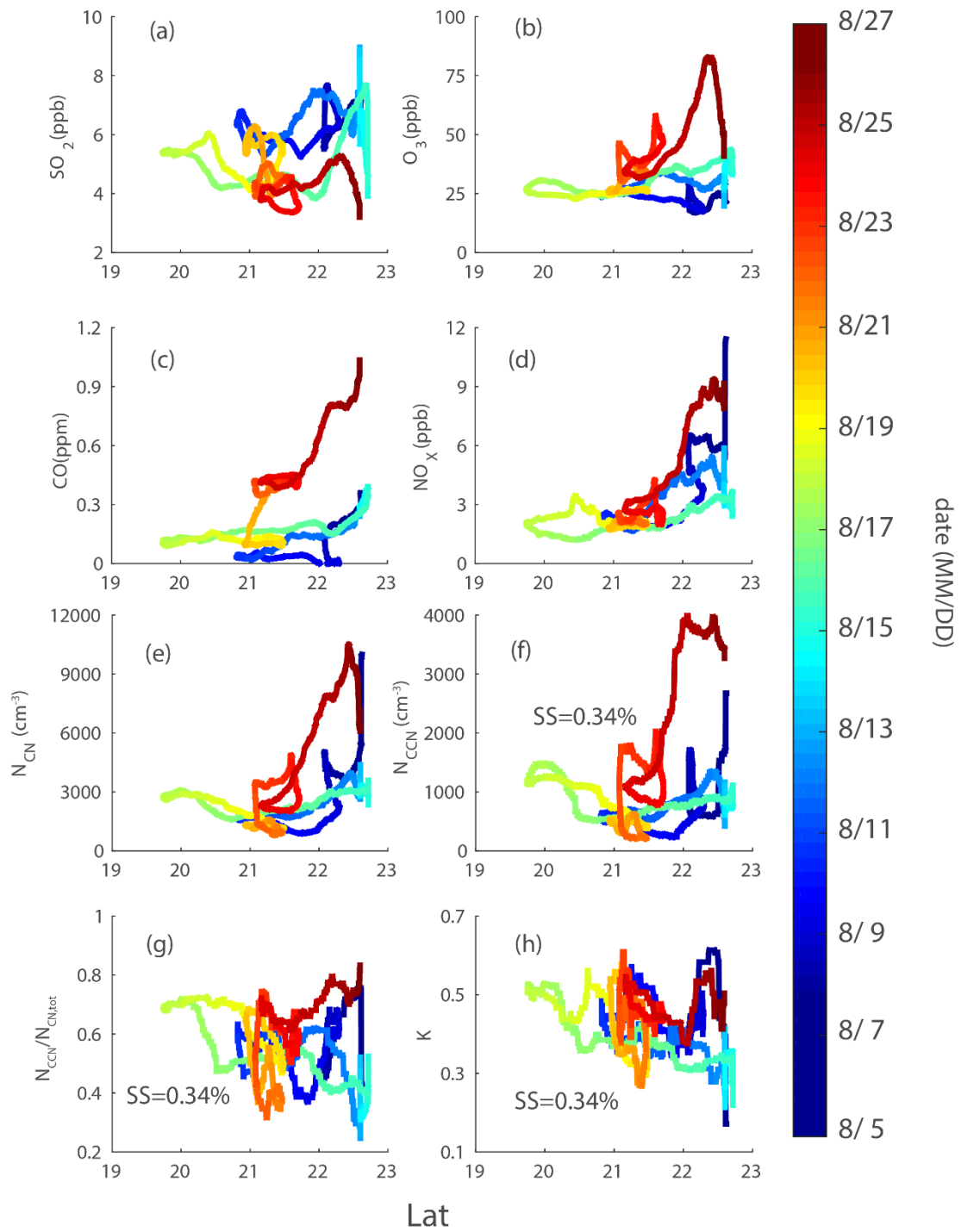


690

691

692 Fig. 3.

693



695

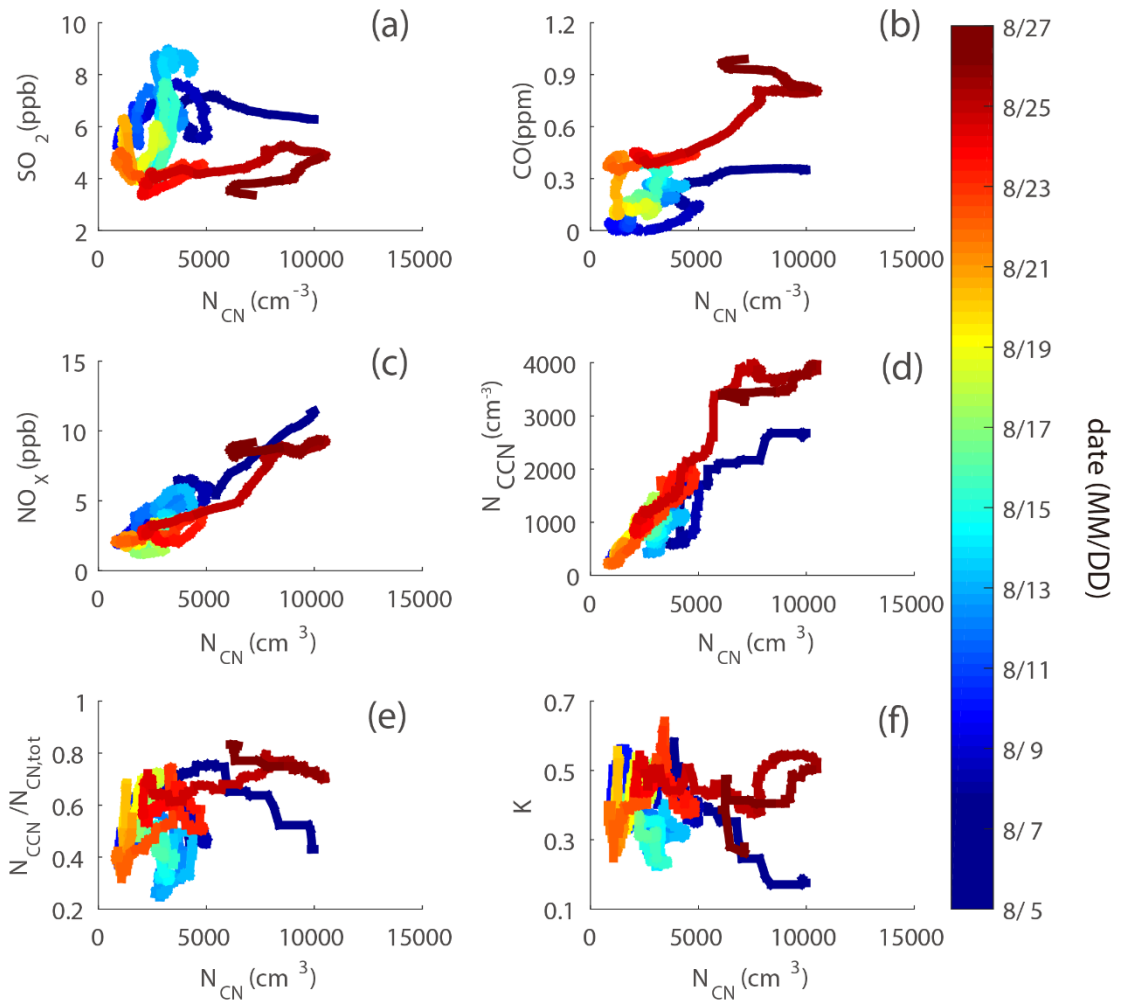
696 Fig. 4.

697

698

699

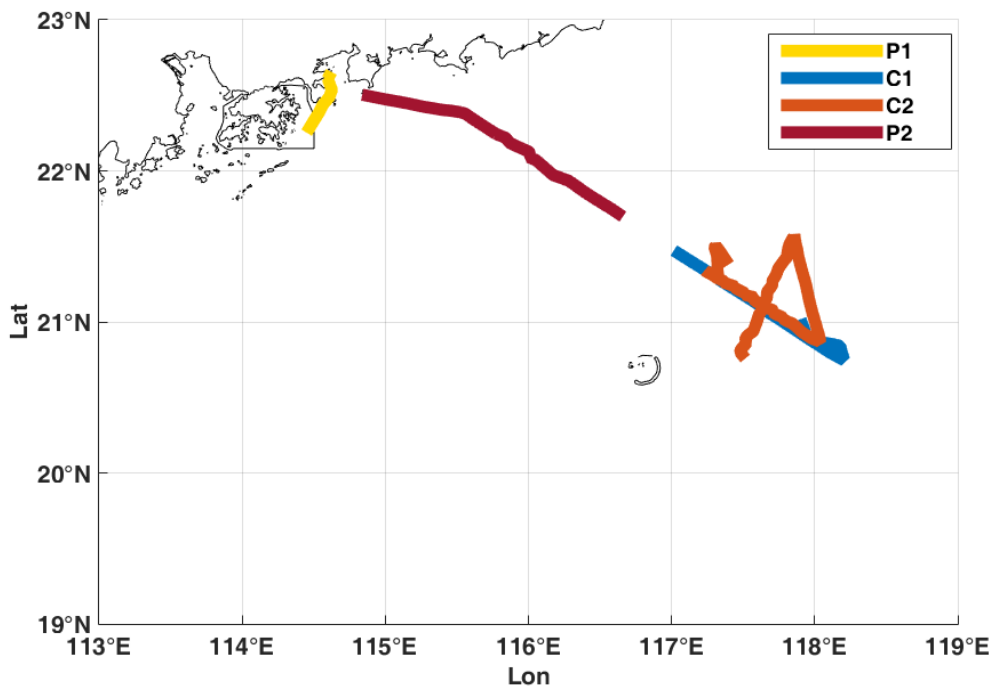
700



701

702 Fig. 5.

703

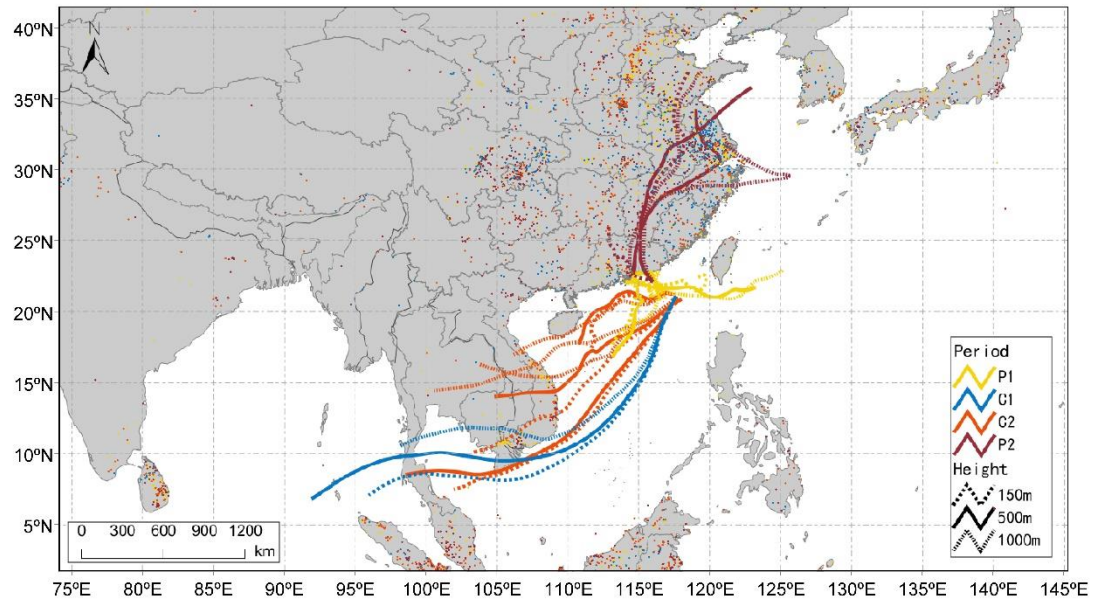


704

705

706 Fig. 6.

707

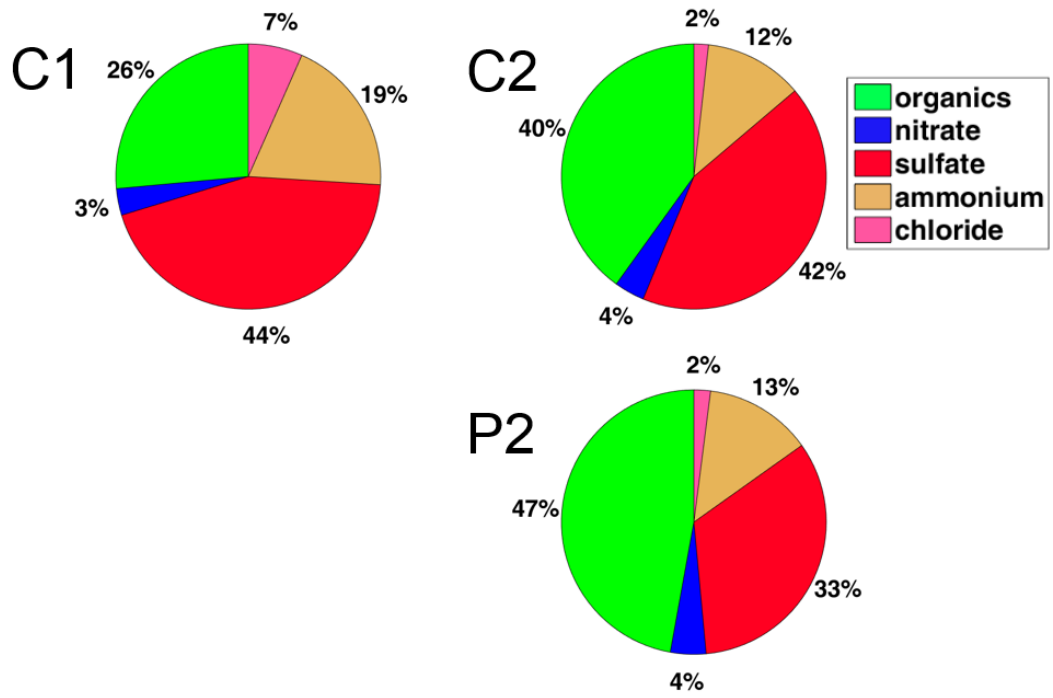


708

709

710 Fig. 7.

711

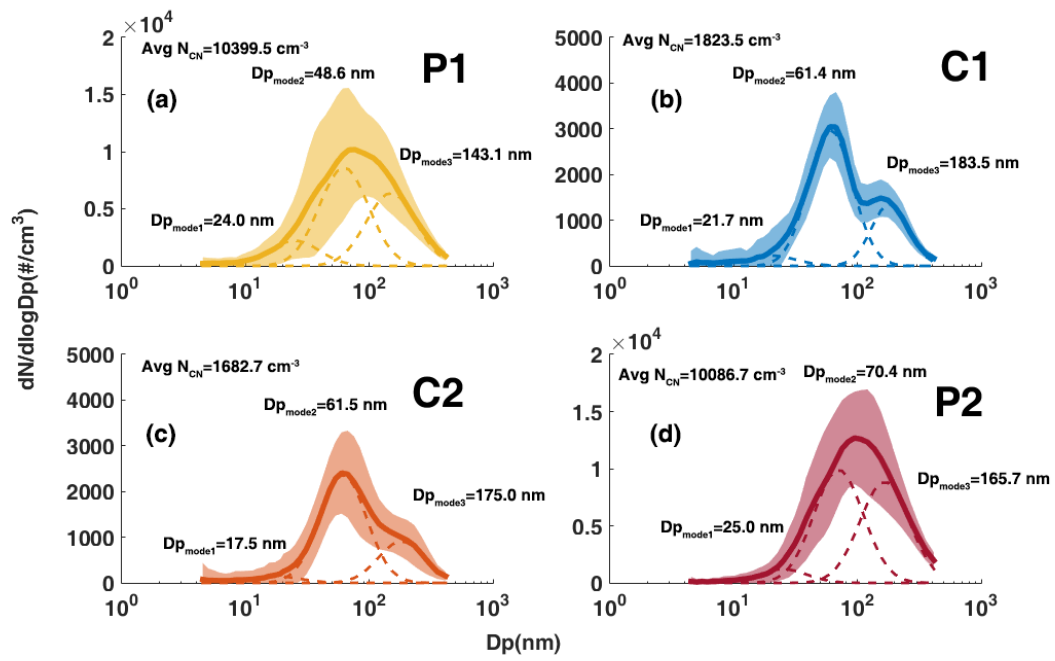


712

713

714 Fig. 8.

715



716

717

718 Fig. 9.

719